BURNOUT RESISTANCE OF CONCRETE STRUCTURES UNDER NATURAL FIRES

by

Jiaqing Pei

A thesis submitted to Johns Hopkins University in conformity with the requirements for the degree of Master of Science

Baltimore Maryland

May 2021

Abstract

The current fire resistance design strategy for concrete structures is based on the consideration of a monotonically increasing fire exposure such as ISO 834. However, this rating method fails to address the possibility of structural collapse in the cooling phase, which can have disastrous consequences for fire fighters and severe socio-economic impacts. To complement this shortcoming, the concept of burnout resistance was proposed to quantify the ability of concrete members to survive full burnout under real fires exposure.

In this research, the relationship between burnout resistance, standard fire resistance and the cooling phase is analyzed for reinforced concrete columns, beams and walls. A standardized natural fire model is first proposed based on the Eurocode parametric fire model for burnout resistance analysis which includes a uniform heating phase and a linear cooling phase with realistic cooling rates. Burnout resistance analysis is performed on several standard fire tests and designs. Finite element modeling, including thermal and mechanical modeling, is applied and calibrated to reproduce available standard tests. Then, the members are analyzed under the proposed standardized natural fire model. An iterative computational procedure is applied to subject each member to increasing durations of fire exposure until finding the shortest standardized fire that cannot be survived until burnout, from which the burnout resistance metrics is defined. Finally, a simple equation is formulated for concrete columns, beams and walls respectively to estimate the burnout resistance from the fire resistance and cooling phase. Such equations can support design for complete burnout which has benefits for safety of fire departments, as well as for property protection and resilience of the built environment.

The results presented in this work show that the cooling phase has a great influence on the burnout resistance. The difference between burnout resistance and traditional fire resistance, which is influenced by the cooling rate, is a good indicator of the possibility of delayed failure. Simple fire severity concepts were explored based on time equivalency or temperature distribution, but these simple methods cannot capture all the complex phenomena affecting burnout resistance of the members, revealing the need for conducting thermal-structural analyses.

The research work presented in this thesis has been supported by the ACI Foundation through research grant # CRC 2020 P0039 awarded to Dr. Thomas Gernay.

Primary Reader and Advisor: Prof. Thomas Gernay

Secondary Reader: Prof. Benjamin W. Schafer

Acknowledgement

I would like to thank Dr. Thomas Gernay for his guidance, leadership, and time dedicated during this project and for giving me the opportunity to conduct this research. I would also like to thank Dr. Ben Schafer for his advice, comments and recommendations and for serving as an additional reader.

I would like to thank my mother, Xin Chen for supporting me throughout my college career and inspiring me to be a better scholar. I would like to thank my best friends Jinlei Xie and Jiaxuan Wen. Without their support, patience, and understanding this project would not have been possible.

I would like to thank my grandmother Ronglan Xu for her inspiration as well as being such a wonderful part of my life. Most importantly, I would like to thank my father Huashan Pei for being my mentor and giving me inspiration throughout my entire life. To you I owe everything.

The support of the ACI Foundation through research grant # CRC 2020 P0039 awarded to Dr. Thomas Gernay is gratefully acknowledged.

Table of Content

List of Tables

List of Figures

1. Introduction

1.1 State of the Art

Fire resistance (R) is an important property in structural fire engineering. It is defined as the duration of time over which a structure fulfills its predefined criteria in terms of its structural integrity, stability, and temperature transmission when exposed to a monotonically increasing standardized fire curve such as ISO 834 [1] or ASTME 119 [2] (see figure 1-1). It provides a standardized way of comparing the performance of structural members exposed to fire in practical structural design. Therefore, this method of assessing the performance of fire exposed structures has been adopted in many design codes for several decades and the information it provides is deemed as sufficient in a prescriptive environment.

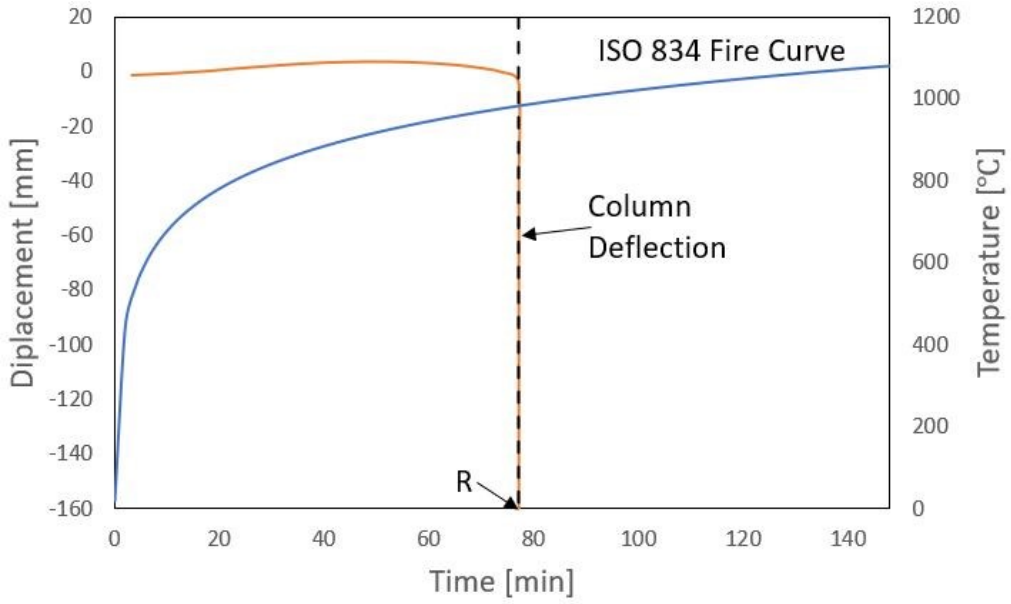

Figure 1-1 - Behavior of a hypothetical column under the standard ISO 834 fire curve and the definition of standard fire resistance [R]

Recently, performance-based objectives for the built environment under extreme hazards are extending from the life safety of building occupants to broader resilience requirements. It is righteously a societal expectation that, in case of disaster, first responders can intervene safely and the building can remain to stand, and even possibly re-occupied after the event. However, meeting these expectations for fire hazard requires complementing the current fire-resistance rating system with a shift in paradigm, since the current design methods are based on an oversimplification of the time-temperature exposure. Apart from a heating phase, realistic compartment fires are also characterized by a cooling phase. Due to the fact that the maximum temperatures in the section can be reached long after the heating phase, delayed failure can happen in structures, especially reinforced concrete structures. While the traditional fire resistance aims at ensuring that buildings remain stable for sufficient time to allow evacuation, it does not contemplate the issue of structural integrity during and after the cooling phases of the fire. This is a significant shortcoming because the current fire designs fail to address the possibility of structural collapse after the time of peak gas temperature under real fires. Such delayed collapses can have disastrous consequences for firefighters and severe socio-economic impacts in the aftermath of the event. For example, in 2004, a delayed failure occurred in the collapse of an underground car park in Gretzenbach, Switzerland. The cast-in-place concrete flat slab structure collapsed in punching shear during the cooling phase after a fire of limited severity [3] . Therefore, it is important to propose a new fire resistance rating metrics, burnout resistance, to quantify the ability of concrete members to survive until full burnout under real fire exposure.

The burnout resistance of a member can be defined as the shortest fire that the member cannot survive through the full burnout. This shortest fire can be standardized in terms of

the shortest Duration of Heating Phase (DHP) of the design natural fires [4] (see figure 1-2). In other words, the member can be subjected to fires of increasing duration of heating phase, until finding the fire that leads to failure. This is an iterative process, easily implemented in a numerical framework. Simulations are run until the very end of the fire when the temperature in the profiles comes back to ambient so that possible failures in cooling or thereafter are duly captured. The standard fire resistance is also computed to explore the relationship with burnout resistance. Since 2019, this approach has been employed for RC columns [5] , RC slabs [6] , and timber columns[7] , showing the applicability of the method.

It is believed that the introduction of this new metrics alongside the fire resistance R can provide a significant improvement to the century-old rating system by accounting for the full course of a fire until burnout, while maintaining the simplicity and efficiency of a prescriptive rating system.

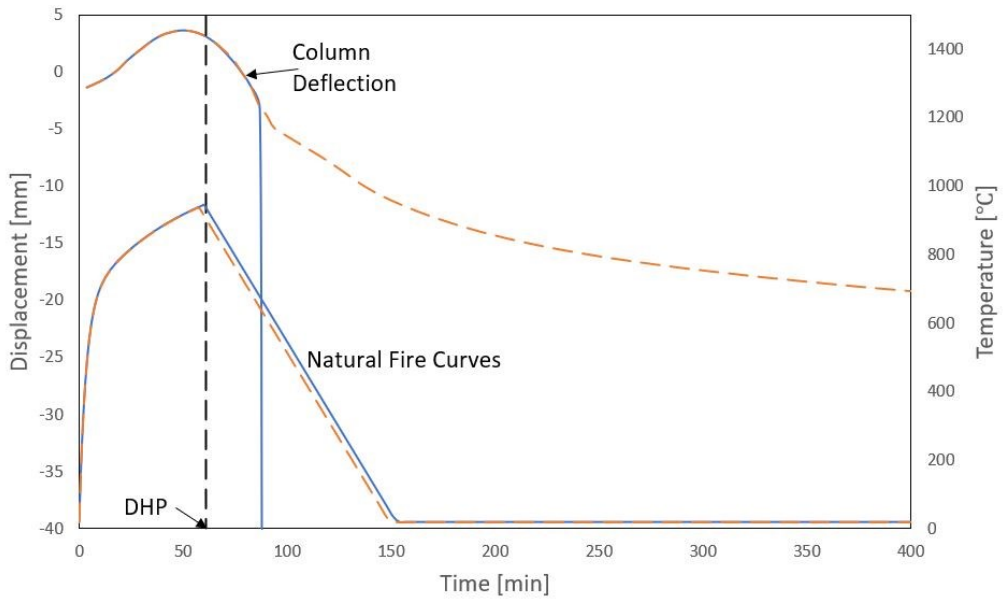

Figure 1-2 - Behavior of a hypothetical column under two standardized natural fire curves and the definition of burnout fire resistance [DHP]

1.2 Research Motivation

The focus of this study is to analyze reinforced concrete structural members under a 'standardized' natural fire model until failure, to observe the influence of the cooling phase on the burnout resistance, and to investigate the relationship between standard fire resistance, cooling rates and burnout resistance. Furthermore, the concept of fire severity will be explored to find a relationship between the different fire exposures that have the same effect on the member. In the end, a simple equation will be developed to predict the burnout resistance of a concrete member from its traditional standard fire resistance and the cooling rate of the applied natural fire. To achieve this purpose, this thesis is organized as follows:

Chapter 1 underlines the importance of quantifying the ability of concrete members to survive until full burnout under real fires exposure, defines the burnout resistance to complement the possibility of delayed failure, and state the objectives of this thesis.

Chapter 2 introduces the formulation of the standardized natural fire model. It starts by modeling various compartment fires in OZone to identify the characteristics of the cooling phases. A parametric analysis is performed to estimate the realistic range of cooling rates for compartment fires. The validity of this range is confirmed by comparing the modelled cooling rates with several tested cooling rates. In the end, a standardized natural fire model based on the Eurocode parametric natural fire model is proposed for the burnout resistance analyses conducted thereafter.

Chapter 3 describes the burnout resistance calculation method based on iterative finite element analyses in the software SAFIR.

Chapter 4 presents the burnout resistance analysis of concrete columns. A database of 74 columns is used in the study, for which standard fire resistance test results are available. Then, the numerical simulations of the 74 columns under both standard fire and natural fires are modeled in SAFIR to calculate the standard fire resistance (R) and burnout resistance (DHP) of the test columns. Fire severity is also applied to seek the relationships between fire exposures and establish a simplified calculation method for the burnout resistance based on the numerical dataset.

Chapter 5 presents the burnout resistance analysis of concrete beams. The research is performed on a column tested in a standard fire resistance test and another column designed based on ACI codes. Then, the numerical simulations under both standard fire and natural fires are modeled in SAFIR to calculate the standard fire resistance (R) and burnout resistance (DHP). Fire severity is also applied to seek the relationships between fire exposures. A simple calculation method for the burnout resistance is derived based on the numerical dataset.

Chapter 6 presents the burnout resistance analysis of concrete wall. A standard fire test of a high-rise RC wall is used in the study. Following the same methodology as in the previous chapter, numerical simulations under both standard fire and natural fires are modeled in SAFIR to calculate the standard fire resistance (R) and burnout resistance (DHP), and a simple calculation method for the burnout resistance is derived based on the numerical dataset.

Finally, Chapter 7 summarizes and draws conclusions about the new developments proposed in this thesis.

2. A Standardized Natural Fire Model

The burnout fire resistance analysis first requires selecting realistic yet simple design natural fire models that include the decay phases and are adequate for burnout resistance design. These models need to encompass the different phases of real fires, yet at the same time be 'standard' so they can be used efficiently to compare alternative structural solutions. The use of the Eurocode parametric fire model has been suggested with a heating phase that approximates the standard ISO 834 curve ($\Gamma = 1$) for a certain duration followed by a linear cooling phase[5] . This approach is promising but still needs to be refined. This model assumes the duration of the heating phase and the cooling rates are dependent. However, the cooling rates can be influenced by various factors including opening factors, properties of the boundary of enclosure, and the possible intervention of fire brigades and it should be mentioned that the cooling rates influence the delayed failures[5] . Therefore, it is necessary to take the cooling rate as an independent factor in the standardized natural fire model. The objective of this chapter is to refine the Eurocode parametric fire model by contemplating the effect of cooling rate on the burnout resistance.

2.1 Investigation of Cooling Rates in Natural Fires

The cooling phase is a major difference between a natural fire and standard fire such as ISO 834. In Eurocode, the cooling phase is expressed as a straight line that decrease from the peak gas temperature to the ambient temperature. The slope of the line is the cooling rate (K). In order to propose a standardized natural fire model, it is necessary to confirm the realistic range of cooling rates. In this section, various compartment fires are modeled in Ozone to identify the characteristics of the cooling phase. To investigate the realistic

range of cooling rate, a parametric analysis is performed to estimate the realistic range of cooling rates for compartment fires. The validity of this range is confirmed by comparing the modelled cooling rates with several cooling rates calculated from Epernon Fire Tests.

2.1.1 OZone Study

OZone is a software developed at University of Liège that helps engineers to model different types of compartment fires [8] [9] . Zone models are used in this software to evaluate the development of the gas temperature within a compartment during a fire. The basic hypothesis of zone models is that the compartment can be divided into zones where each zone has a uniform temperature distribution at any time. In single-zone models, the temperature is considered uniform in the whole compartment. This type of model is usually used for fully developed fires. In two-zone models, there is a hot gas layer which is close to the ceiling and a cold gas layer which is close to the floor. Thus, two-zone models are normally used for localized fires or the pre-flashover phase. This software also includes a model to switch from the two-zone to the one-zone model. In this study, a two-zone model is used for the pre-flashover phase and a single-zone model is then used for the fully developed phase. The fire curve is taken as the development of gas temperature.

By defining the geometry of the compartment and the properties of fire, the time-temperature relationship for the fire can be easily calculated. In this study, the compartment is made of normal weight concrete according to EN 1994-1-2[10] and the occupancy is defined as dwelling. The input data are shown in Table 2-1. Parametric analyses are conducted to investigate the influence of factors on the cooling rate, including floor area (S), height (h), opening factor (O), and the thickness of gypsum board (t). The opening

factor describes the ventilation condition of a compartment and is expressed as Eq. 2-1 in Eurocode 1991-1-2[11] :

$$O = A_v\sqrt{h_{eq}}/A_t \quad (2\text{-}1)$$

with the following limits: $0.02 \leqslant O \leqslant 0.2$, where

A_v: total area of vertical openings on all walls [m^2]

h_{eq}: weighted average of window heights on all walls [m]

A_t: total area of enclosure (walls, ceiling and floor, including openings) [m^2]

Table 2-1 – Input data of OZone

Parameters	Value
Material	Normal weight concrete (EN 1994-1-2)
Occupancy	Dwelling
Floor area (m*m)	3*3, 4*4, 5*5, 6*6, 8*8,10*10
Opening factors ($m^{1/2}$)	0.02-0.16
Height (m)	2.5-4
Thickness of gypsum board (cm)	0-2.5

Figure 2-1 plots the fire curves of an 8*8*3 m^3 compartment with different opening factors modeled by OZone. It is observed that the cooling phase of a compartment fire is characterized by two branches. The gas temperature starts to rapidly drop below 400 ℃ once it reaches the highest temperature and a then slowly drops to the ambient temperature. Both branches can be idealized as a linear decline phase. Since the delayed failure usually occurs during the rapid decline phase, the cooling rate K is taken as the slope of the rapid decline phase in the proposed natural fire model.

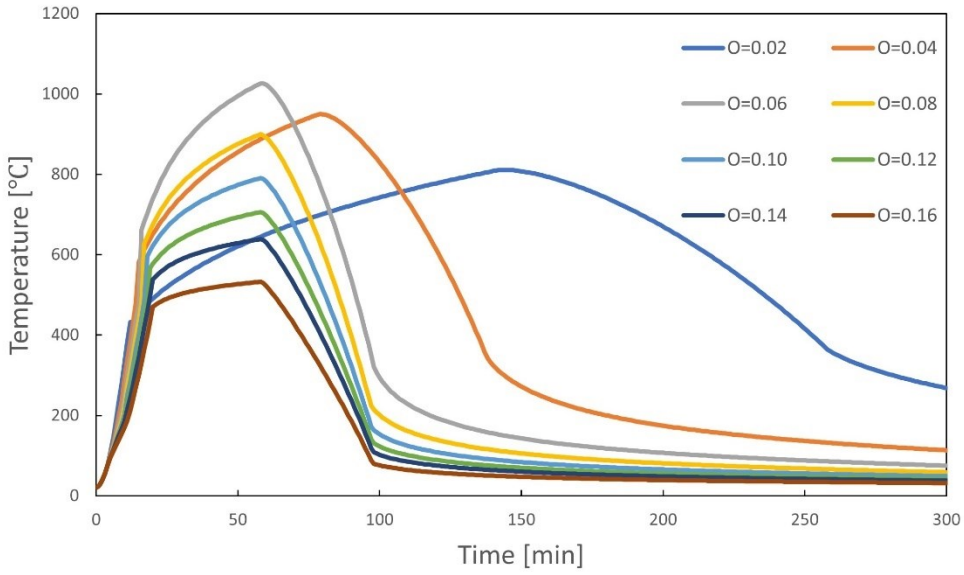

Figure 2-1 - Fire curves of an 8-8-3 compartment with several opening factors modeled by OZone

Figure 2-2 shows the relationship between cooling rates and opening factors for a compartment with different floor areas. The cooling rate increases with the opening factor at first, but there is a turning point which is around 0.04 or 0.06. When the opening factor exceeds that point, the cooling rate gradually decreases (because the peak temperature decreases for over-ventilated fires, see Figure 2-1). We can get the minimum K when O=0.02 and the maximum K when O=0.04 or 0.06. The floor area also influences the value of K, K tends to have a larger variance when the compartment has a larger floor area.

Figure 2-3 shows the relationship between the cooling rates and the compartment height for a compartment with a floor area of 6m-6m. The influence of compartment height on K depends on the value of opening factors. When the opening factor is small, increasing the compartment height will slightly increasing the value of K. However, when the opening factor increases to a certain value around 0.06 for this case, increasing the compartment height will slightly decrease K.

The influence of the presence of gypsum board on the cooling rate is shown in figure 2-4. To investigate this influence, gypsum board layers with different thickness are placed on the ceiling and walls. The results show that the presence of gypsum board would increase the value of K and K will also increase with the thickness of the gypsum board.

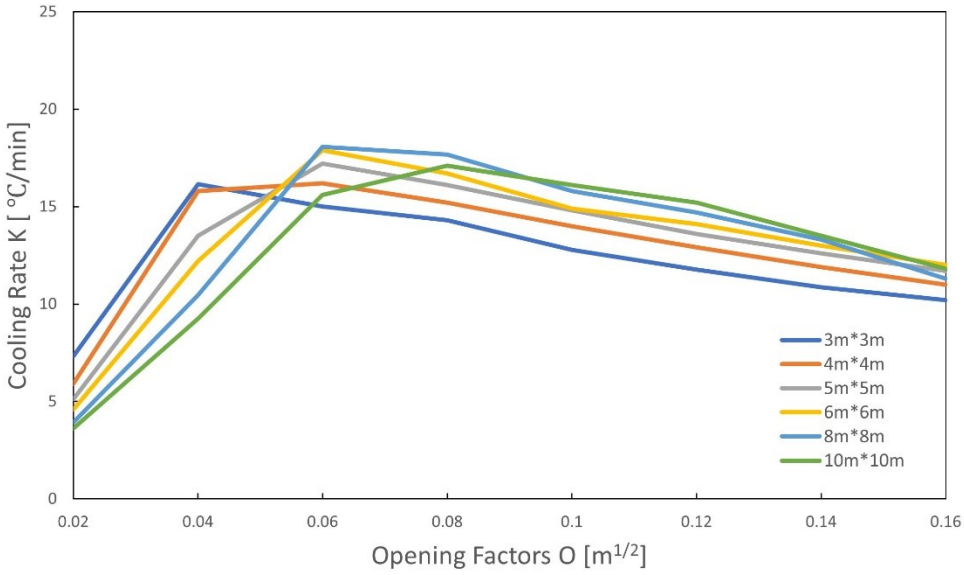

Figure 2-2 - Cooling rate – Opening factor relationship

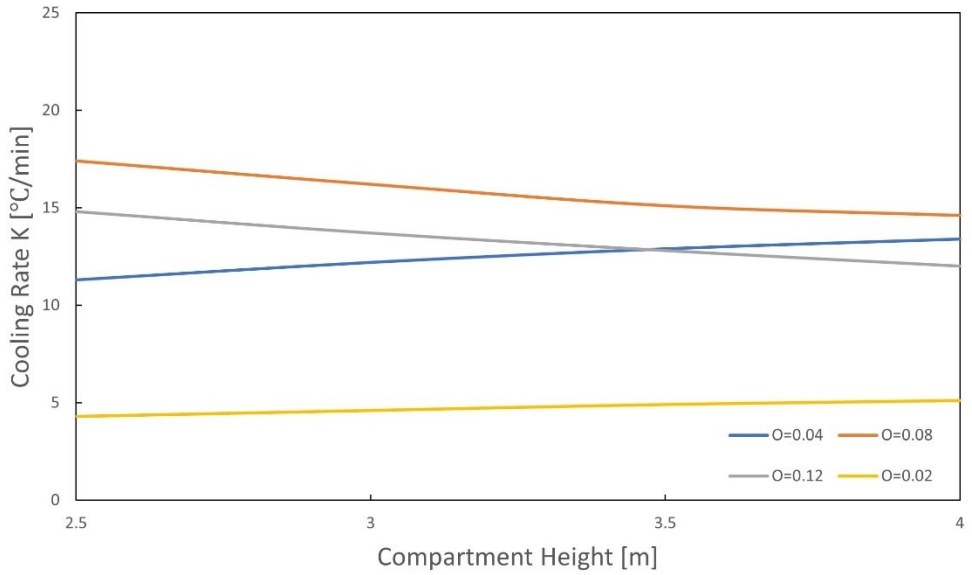

Figure 2-3 - Cooling rate - compartment height relationship for a compartment with floor area of 6m*6m

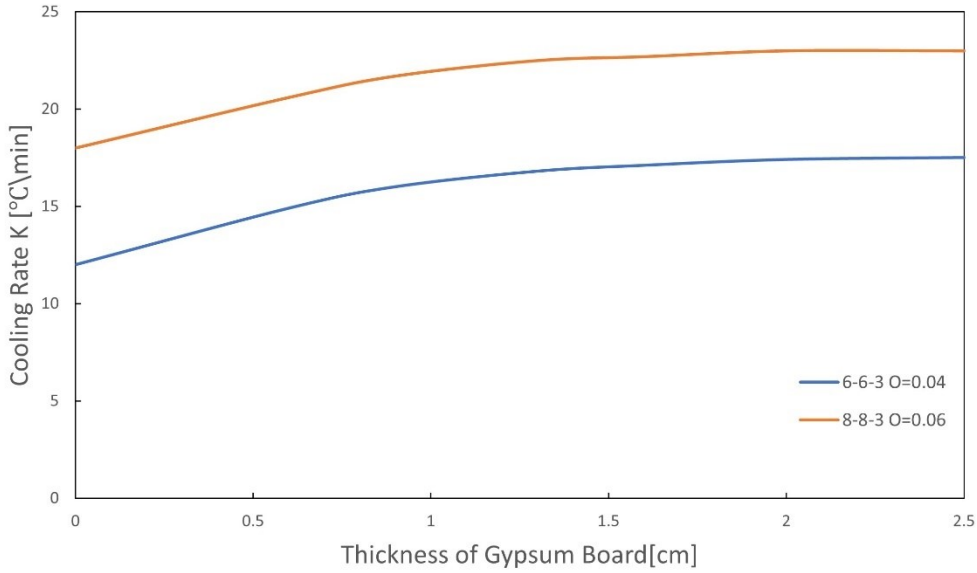

Figure 2-4 - Cooling rate - thickness of gypsum board relationship for two types of compartments

In summary, the cooling phases of compartment fires can be idealized as a straight line with a slope of K. The magnitude of K can be influenced by various factors including the compartment size, the ventilation condition and the presence of gypsum boards. The

opening factor (O) controls the value of K. When O is around 0.05, K is at its peak value. In this OZone study, the range of K can be taken from 2 ℃/min to 20 ℃/min.

2.1.2 Épernon Fire Tests Validation

This section aims to validate the range of K generated from Ozone by comparing the Ozone results with the cooling rates calculated from Épernon fire tests. "The Épernon Fire Tests Program" is a project that seeks to understand the links between normative fire resistance ratings and real fire performance in buildings[12] . Fire tests includes two different loaded structures, ceiling slabs made of cross-laminated timber (CLT) and ceiling slabs made of reinforced concrete[13] . These two types of slabs were tested in compartment fire experiments with timber cribs as a fuel load. Different opening factors were tested (figure 2-5). The dimension of the compartment is 6 m x 4 m in plan and 2.52 in height. The fire load during the compartment tests was 891 MJ/m² which is representative of the characteristic fire load for dwellings according to EN 1991-1-2 (Annex E) [11] .

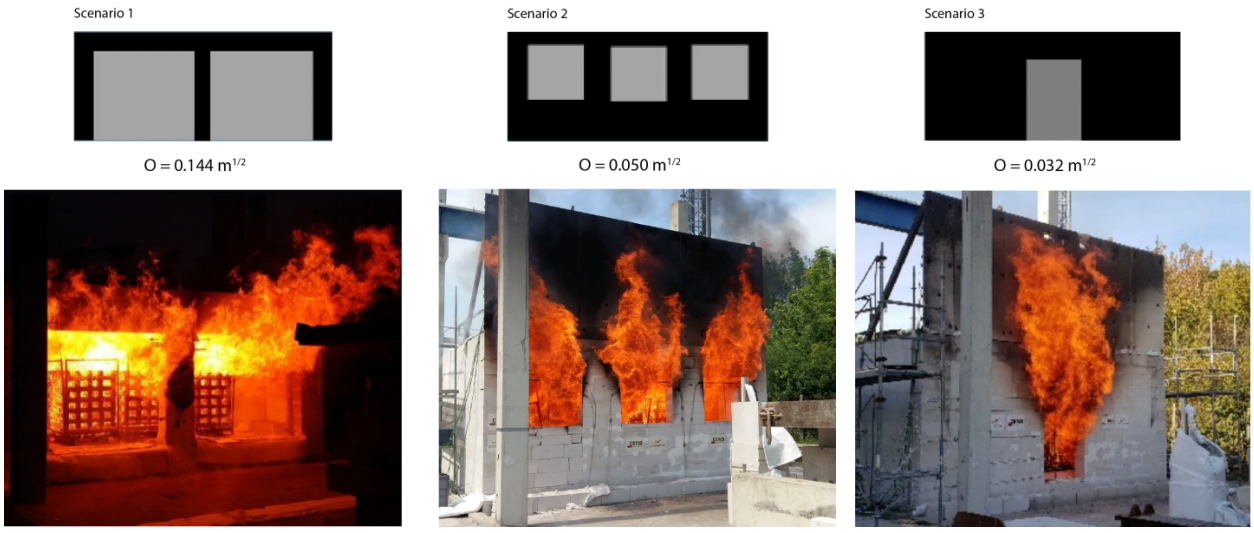

Figure 2-5 - Illustration of compartment configurations and corresponding opening factor.[12]

During the compartment fire experiments, the time-temperature relationships of the fires are recorded (see figure 2-6 and table 2-2). The cooling rate ranges from 6-28 ℃/ min, which exceeds the upper limit of the OZone range. However, the average cooling rate (from beginning to end) is about 10-11 °C/min, which fits well within the 2-20 °C/min range determined by the OZone analysis. Besides, when the cooling rate reaches large values, the impact of an increase in the rate of cooling on the burnout resistance becomes negligible. The results of the burnout resistance analysis in chapter 4 will show that the burnout resistance will reach a plateau when K is around 20 ℃/ min. Therefore, the range of K selected from the OZone study is reasonable.

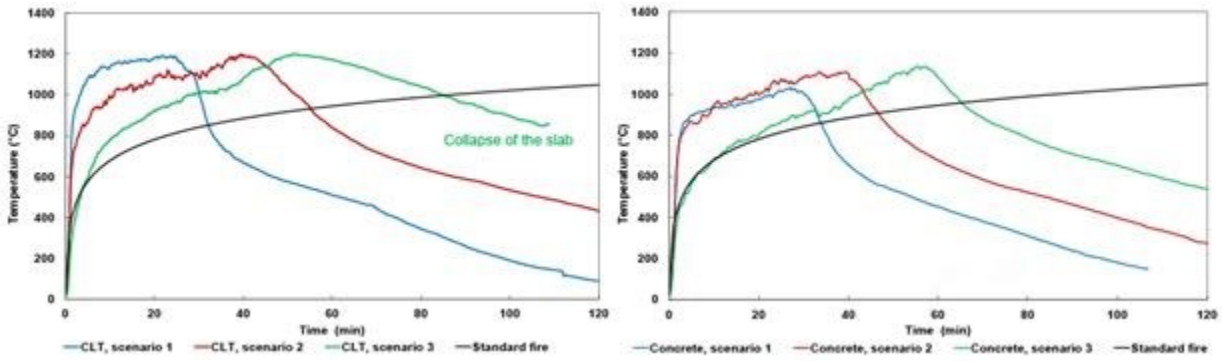

Figure 2-6 - The temperature development inside the compartment for the three different scenarios.[12]

Table 2-2 Cooling rates of the tested compartment fires

Slab material	Cooling rate (℃/min)					
	CLT			Concrete		
Fire scenario	1	2	3	1	2	3
Fast branch	39.53	17.89	6.04	27.57	26.15	16.35
Slow branch	7.7	6.16	6.04	6.79	7.48	6.56
Slope from cooling beginning to ending	11.69	9.78	6.04	11.26	10.38	9.54

2.2 Proposed Natural Fire Model

This section seeks to propose a systematic model to characterize the compartment fires based on Eurocode parametric fire model according to EN 1992-1-2 Annex A [11] . In the Eurocode parametric fire model, the heating phase is expressed as Eq. 2-2 and the cooling phase is expressed as Eq. 2-3. The factored time $t^* = t * \Gamma$ where Γ is a parameter that depends on the opening factor and the thermal properties of the boundary of enclosure. t represents the time in hours and DHP represents the Duration of Heating Phase (DHP) in hours as well. T_{max} is the peak gas temperature in ℃. The Eurocode parametric fire model is valid for fire compartments up to 500 m^2 of floor area, without openings in the roof and for a maximum compartment height of 4 m. It is assumed that the fire load of the compartment is completely burnt out.

$$T=20+1325(1-0.324e^{-0.2t^*} -0.204e^{-1.7t^*} -0.472e^{-19t^*}) \quad (2\text{-}2)$$

$$T=T_{max}-625(t^* -DHP) \quad \text{for DHP} \leqslant 0.5h \quad (2\text{-}3a)$$

$$T=T_{max}-250(3-DHP)(t^* -DHP) \quad \text{for } 0.5h<DHP<2h \quad (2\text{-}3b)$$

$$T=T_{max}-250(t^* -DHP) \quad \text{for DHP} \geqslant 2h \quad (2\text{-}3c)$$

To use a systematic method to characterize the fire burnout resistance, the standardized natural fire is defined as the Eurocode parametric fire model with $\Gamma = 1$. When setting $\Gamma = 1$, this compartment fire model has an opening condition that makes its heating phase approximate the ISO 834 standard temperature-time curve. The linear cooling phase depends on the duration of heating phase. Therefore, the model has only one parameter, the Duration of Heating Phase (DHP). The temperature-time curve in the heating phase is

given by Eq. (2-4). The temperature-time curves in the cooling phase are given by Eq. (2-5a), (2-5b) and (2-5c). Figure 2-7 shows the fire curves generated from the Eurocode parametric fire model with $\Gamma = 1$.

$$T=20+1325(1-0.324e^{-0.2t} -0.204e^{-1.7t} -0.472e^{-19t}) \quad (2\text{-}4)$$

$$T=T_{max}-625(t -DHP) \quad \text{for DHP} \leqslant 0.5h \quad (2\text{-}5a)$$

$$T=T_{max}-250(3-DHP)(t -DHP) \quad \text{for } 0.5h<DHP<2h \quad (2\text{-}5b)$$

$$T=T_{max}-250(t -DHP) \quad \text{for DHP} \geqslant 2h \quad (2\text{-}5c)$$

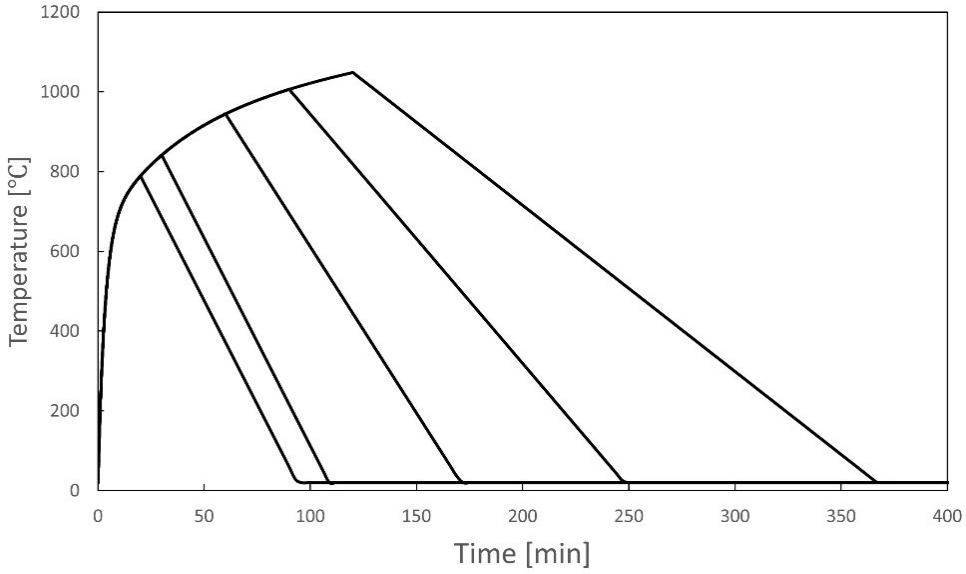

Figure 2-7 - Examples of Eurocode parametric fire curves when $\Gamma=1$

To refine the Eurocode parametric fire model to contemplate the impact of cooling phase, the cooling rate is taken as an independent factor (K in °C/h) in the proposed standardized natural fire model. The heating phase remains the same. From Section 2.1, the value of K should be between 120 °C/h and 1200 °C/h. Figure 2-8 shows the fire curves generated from the proposed fire model. The refined model has two independent parameters (DHP

and K). For instance, the curve 'DHP=20 min, K=2 °C/min' represents a fire curve with a heating phase of 20 min duration and a cooling rate of 2 C/min (120 °C/h).

Compared with the Eurocode natural fire model, this refined model can capture the cooling phase more directly, for instance, the cooling rate is a constant value (625 °C/h) when DHP is 30 min in the Eurocode natural fire model. This makes engineers fail to evaluate the structural performance under a compartment fire with a different cooling rate like 300 °C/h or 900 °C/h that also might occur in the designed compartment. This problem can be easily solved by adopting the refined fire model. Engineers can evaluate the performance of a structure under natural fires with all the possible cooling rates. This model is expressed as Eq. 2-6 and 2-7:

$$T=20+1325(1-0.324e^{-0.2t}-0.204e^{-1.7t}-0.472e^{-19t}) \quad (2\text{-}6)$$

$$T=T_{max}-K(t-DHP) \quad (2\text{-}7)$$

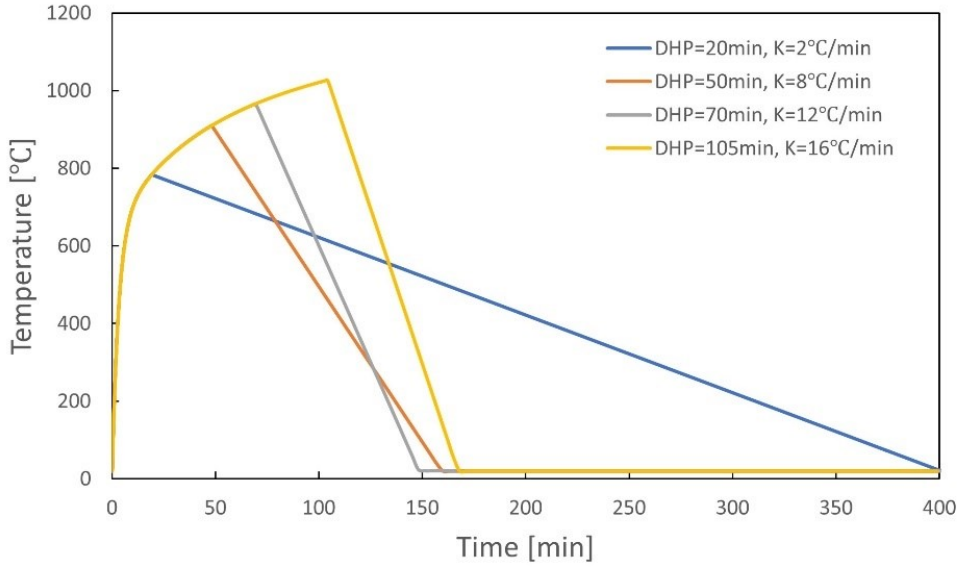

Figure 2-8 - Examples of proposed natural fire curves

3. Burnout Resistance Calculation Method

Calculating the DHP of a concrete component under a given load is a more complex operation than calculating the traditional fire resistance. Searching for the DHP of a component is to search for the shortest design fire curve that will eventually leads to the failure of the component. The process is thus iterative where temperature-time curves of increasing duration of heating phase are applied to the component until reaching failure. Because of the iterative procedure, experiments are not applicable in practice. Numerical models must be used, where the behavior of the component under heating-cooling is evaluated through nonlinear thermal-structural finite element analyses.

A half interval search method is used for this process to reduce iterative times. The iterative process can be automatized as according to the flowchart of figure 3-1. A Matlab script is created based on this flowchart for burnout resistance analysis. A fire is first selected based on its duration of heating phase (in min) and cooling rate K (in °C/min). For a given fire, a thermal analysis is run, followed by a mechanical analysis. Structural failure can occur during or after the cooling phase under a natural fire. Therefore, the analyses are run for long enough past the time when the gas temperature is back to ambient. The thermal effects are thus completely dissipated and we can ascertain that there is no failure for such natural fire. If no failure is occurred, the duration of the heating phase of the fire is slightly increased and the analyses are repeated.

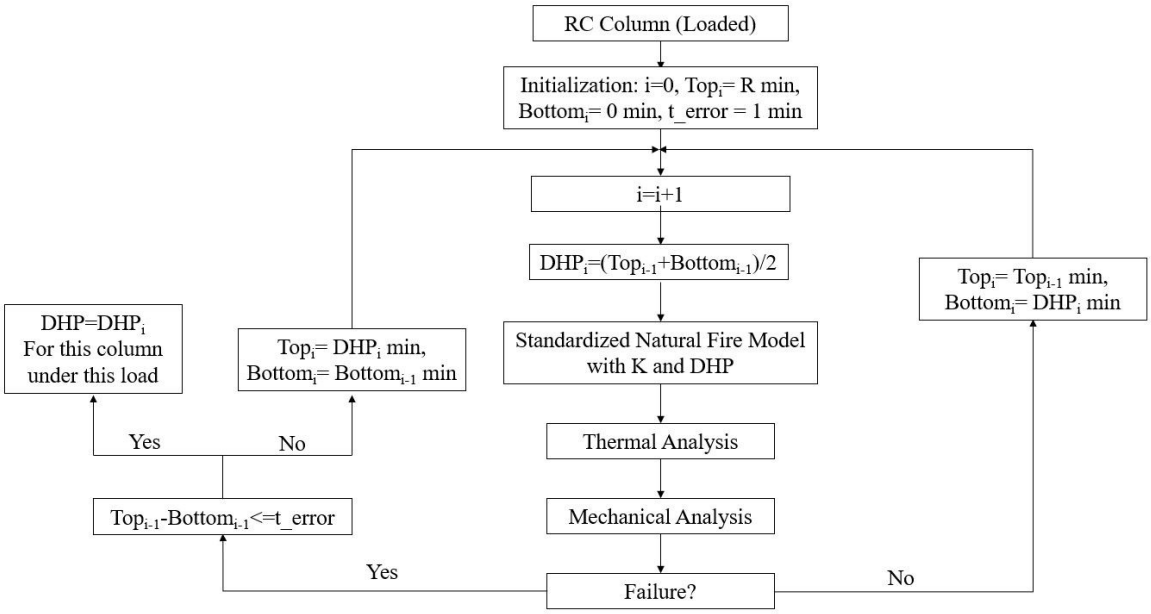

Figure 3-1 - Flowchart of the iterative procedure to obtain the DHP of a reinforced concrete column under a given applied load.

4. Burnout Resistance of Concrete columns

4.1 Test Database

74 fire resistance tests of concrete columns are used for burnout resistance analysis in this report. 39 tests were conducted at the Technical University of Braunschweig in Germany (TUBr) [14] , 12 tests were conducted at the University of Ghent in Belgium (RUG) [15] , 4 tests were conducted at the University of Liege in Belgium (ULg) [15] , and 19 tests were conducted at the National Research Council in Canada (NRC) [16] . In each of the 74 tests, a loaded reinforced concrete column was exposed to a standard temperature-time curve on its four sides. The tests conducted in Europe used the ISO 834 thermal exposure while the tests conducted in Canada used the ASTM-E119 (ULC-S101), which is very similar.

The data are presented in Table 4-1. Parameters vary between the tests including the boundary conditions, length of the columns, cross sections, reinforcement ratio, material strengths, and magnitude and eccentricity of the load. In Table 4-1, L is the length of the tested columns, h and b describe the height and width of the cross-section. The n and Φ correspond to the number and diameter of longitudinal reinforcement bars in the section, and c is the cover to the edge of the rebar. The eccentricity of the applied load N is given by e_0. The value f_{cm} is the mean cylindrical compressive strength of concrete at the date of the fire test. The value f_{ym} is the mean yield strength of the reinforcement steel. Most of the 39 columns tested at TUBr were hinged at both ends (pinned-pinned), with some hinged at one end and clamped at the other (fixed-pinned). All the columns tested in Ghent and Liege were hinged at both ends (pinned-pinned). Most of the 19 columns tested at NRC

were clamped at both ends (fixed-fixed), which led to longer fire resistances (beyond 3 h). The eccentricity of the load N is given by e0.

Table 4-1 - Experimental database of the standard fire resistance test on reinforced concrete columns (from[5])

#	Lab[a]	L	Ends[b]	h	b	n	Φ	c	e_0	f_{cm}	f_{ym}	N	R test
		m		mm	mm		mm	mm	mm	Mpa	Mpa	kN	min.
1	TUBr	3.76	a	300	300	6	20	28	30	24.4	487	710	86
2	TUBr	3.76	a	300	300	6	20	28	0	24.4	487	930	84
3	TUBr	3.76	a	300	300	6	20	28	0	24.4	487	930	138
4	TUBr	4.76	a	300	300	6	20	28	30	24.4	487	650	63
5	TUBr	4.76	a	300	300	6	20	28	0	24.4	487	880	108
6	TUBr	5.76	a	300	300	6	20	28	30	24.4	487	600	61
7	TUBr	5.76	a	300	300	6	20	28	0	24.4	487	800	58
8	TUBr	3.76	a	200	200	4	20	28	0	24.4	487	420	58
9	TUBr	3.76	a	200	200	4	20	28	0	24.4	487	420	66
10	TUBr	4.76	a	200	200	4	20	28	0	24.4	487	340	48
11	TUBr	4.76	a	300	300	6	20	28	30	31.1	462	650	80
12	TUBr	4.76	a	300	300	6	20	28	30	31.1	462	650	69
13	TUBr	4.76	a	300	300	6	20	28	15	31.1	462	740	85
14	TUBr	4.76	a	200	200	4	20	28	10	31.1	462	280	49
15	TUBr	4.76	a	200	200	4	20	28	20	31.1	462	240	36
16	TUBr	4.76	a	300	300	6	20	28	90	31.1	462	460	75
17	TUBr	4.76	a	300	300	6	20	28	150	31.1	462	360	65
18	TUBr	4.76	a	200	200	4	20	28	60	31.1	462	170	49
19	TUBr	4.76	a	200	200	4	20	28	100	31.1	418	130	53
20	TUBr	3.80	b	300	300	6	20	28	30	33.6	458	845	111
21	TUBr	3.80	b	300	300	6	20	28	50	33.6	418	780	125
22	TUBr	5.76	a	200	200	4	20	28	10	32.8	443	208	40
23	TUBr	4.76	b	300	300	6	20	28	15	31.1	433	735	160
24	TUBr	4.76	b	300	300	6	20	28	150	43.7	544	355	89
25	TUBr	4.76	a	300	300	6	20	28	15	31.9	499	735	93
26	TUBr	4.76	a	300	300	6	20	28	30	38.6	449	645	135
27	TUBr	4.76	a	300	300	6	20	28	5	38.6	404	1224	48
28	TUBr	3.76	a	300	300	6	20	28	5	42.8	452	1695	57
29	TUBr	4.70	a	300	300	6	20	28	5	35.3	505	1548	38
30	TUBr	4.70	a	300	300	6	14	28	10	31.9	503	970	55
31	TUBr	4.70	a	300	300	6	20	28	10	31.9	526	1308	57
32	TUBr	4.70	a	300	300	6	14	28	150	31.9	503	280	49
33	TUBr	4.70	a	300	300	6	20	28	150	31.9	526	465	50
34	TUBr	5.71	a	200	200	6	14	23	100	42	480	140	31
35	TUBr	5.71	a	200	200	6	14	23	10	42	477	245	40
36	TUBr	5.71	a	200	200	6	14	23	50	42	480	172	35

37	TUBr	5.71	a	200	200	6	14	23	10	42	482	175	49
38	TUBr	5.71	a	200	200	6	14	23	50	42	485	122	52
39	TUBr	5.71	a	200	200	6	14	23	10	42	478	128	72
40	RUG	3.90	a	300	300	4	16	25	0	34.4	576	950	61
41	RUG	3.90	a	300	300	4	16	25	0	35.9	576	622	120
42	RUG	3.90	a	300	300	4	16	25	20	37	576	220	125
43	RUG	3.90	a	300	300	4	16	25	-20	33.8	576	664	128
44	RUG	3.90	a	300	300	4	16	25	0	29.7	576	422	116
45	RUG	3.90	a	300	300	4	16	40	20	37	576	349	123
46	RUG	3.90	a	300	300	4	16	25	20	36.4	576	370	126
47	RUG	3.90	a	400	400	8	16	25	20	30	576	1650	93
48	RUG	3.90	a	200	300	6	12	25	20	31.6	493	300	60
49	RUG	3.90	a	200	300	6	12	25	20	30	493	178	120
50	RUG	3.90	a	200	300	6	12	35	20	32.9	493	283	60
51	RUG	3.90	a	200	300	6	12	35	0	32.8	493	334	120
52	ULg	3.90	a	300	300	4	16	25	0	32.3	576	1270	63
53	ULg	2.10	a	300	300	4	16	25	0	32	576	803	123
54	ULg	2.10	a	200	300	6	12	25	0	33.6	493	611	107
55	ULg	2.10	a	200	300	6	12	35	0	31.6	493	620	97
56	NRC	3.81	c	305	305	4	25.5	48	0	36.9	444	1333	170
57	NRC	3.81	c	305	305	4	25.5	48	0	34.2	444	800	218
58	NRC	3.81	c	305	305	4	25.5	48	0	35.1	444	711	220
59	NRC	3.81	c	203	203	4	20	48	0	42.3	442	169	180
60	NRC	3.81	c	305	305	4	25.5	48	0	36.1	444	1067	208
61	NRC	3.81	c	305	305	4	25.5	48	0	34.8	444	1778	146
62	NRC	3.81	c	305	305	4	25.5	48	0	38.3	444	1333	187
63	NRC	3.81	c	305	305	4	25.5	48	0	43.6	444	1044	201
64	NRC	3.81	c	305	305	4	25.5	48	0	35.4	444	916	210
65	NRC	3.81	c	305	305	4	25.5	48	0	52.9	444	1178	227
66	NRC	3.81	c	305	305	4	25.5	48	0	49.5	444	1067	234
67	NRC	3.81	c	305	305	8	25.5	48	0	42.6	444	978	252
68	NRC	3.81	c	305	305	8	25.5	48	0	37.1	444	1333	225
69	NRC	3.81	c	406	406	8	25.5	48	0	38.8	444	2418	262
70	NRC	3.81	c	406	406	8	32.3	48	0	38.4	414	2795	285
71	NRC	3.81	b	305	305	4	25.5	48	0	39.6	444	800	242
72	NRC	3.81	b	305	305	4	25.5	48	0	39.3	444	1000	220
73	NRC	3.81	a	305	305	4	25.5	48	25	39.9	444	1000	181
74	NRC	3.81	b	305	305	4	25.5	48	25	37.9	444	1178	183

a Lab: TUBr = Braunschweig , RUG = Ghent , ULg = Liege, NRC.

b Ends: a = pinned-pinned, b = fixed-pinned, c = fixed-fixed.

Examination of the data shows that the measured fire resistance varies from 31 min to 285 min for different specimens. The load level is an important factor; the fire resistance

increases when the load decreases. The slenderness ratio also influences the fire resistance, the specimen with higher slenderness ratio generally leads to lower fire resistance.

4.2 Numerical Modeling

The nonlinear finite element software SAFIR is used to compute the thermal and mechanical response of these columns. The program can be used to analyze one to three-dimensional structures under ambient and elevated temperatures. Various elements and material models (linear and nonlinear) are available for the idealization of the structure. Thermal, torsional and structural analysis can be performed either in 2D or 3D. In this section, only 2D analysis were performed using 2D conductive solid elements for the thermal analysis and 2D beam elements for the structural analysis. A detailed description of this software is given in Ref. [17] . The ability of SAFIR to capture the behavior of concrete columns under standard fire exposure has been validated by Gernay [5] using a significant statistical basis. This section reports the numerical simulation of the 74 columns presented in Table 4-1 under the proposed standardized natural fire model.

The inputs of Table 1 are used in the numerical simulations. 'SILCON_ETC' is used for the concrete. In this model, the explicit transient creep formulation [18] is adopted instead of the implicit formulation of the Eurocode. The equivalent cylinder strength f_{cm} is used for the concrete compressive strength while a value of 1/10 of f_{cm} is assumed for the tensile strength. 'STEELEC2EN' is used for the reinforcement and the material is assumed as hot rolled class A. This class of reinforcement is the less ductile with a descending branch starting at a strain of 0.05[19] . The steel reinforcement yield strength is taken as f_{ym}. The material properties are summarized in Table 4-2.

Table 4-2 – Summary of material properties for RC columns simulations

Material Properties		Value
Concrete	Specific Mass [kg/m^3]	2400
	Moisture Content [kg/m^3]	72
	Convection Coeff. Hot [W/m^{2}K]	35
	Convection Coeff. Cold [W/m^{2}K]	4
	Relative Emission	0.7
	Parameter of Thermal Conductivity	0
	Poisson Ratio	0.2
	Compressive Strength [MPa]	see table 4-1
	Tension Strength [MPa]	see table 4-1
Steel	Convection Coeff. Hot [W/m^{2}K]	35
	Convection Coeff. Cold [W/m^{2}K]	4
	Relative Emission	0.7
	Young's Modulus [Gpa]	210
	Poisson Ratio	0.3
	Yield Strength [MPa]	see table 4-1
	Type	Hot-rolled Class A

The calculation process within the program consists of two steps, namely thermal analysis and structural analysis.

The thermal analysis predicts the temperature distribution inside the cross-section while the structure is exposed to fire. The discretization for plane sections is by using triangular elements. For each element, the material can be defined separately, here steel and concrete are predefined. The variation of material properties as well as the evaporation of moisture are considered. The fire exposure is implemented as a function of time and either predefined code temperature curves can be used or other curves, also including a cooling phase, can be modelled. For instance, figure 4-1 shows the discretization of the column cross-section of test 1 using SAFIR thermal analysis. The reinforcements are divided into

8 elements. The results of the thermal analysis can be displayed with the post-processor Diamond, or the data can be evaluated using a text editor.

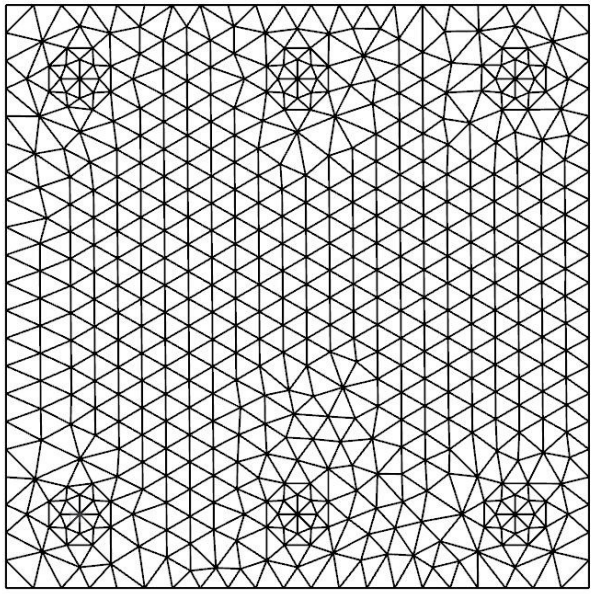

Figure 4-1 - Discretization of the column cross-section of test 1 using SAFIR thermal analysis

The mechanical analysis determines the response of the structure due to static and thermal loading. The test column is idealized as a 2D structure and modeled with beam elements. The calculation is based on a step-by-step procedure integrating the temperature distribution obtained from the thermal analysis at each time step. For each step, the program determines the successive position of equilibrium under the load using an incremental-iterative solver. Buckling is captured as the software accounts for large displacements and geometrical nonlinearities. However, spalling is not taken into account. During the cooling phase, concrete, which is cooling down to ambient temperature after having reached a high temperature during a fire, does not recover its initial compressive strength. Furthermore, it exhibits an additional loss of strength compared to the value at maximum reached temperature, i.e. additional degradation occurs during cooling [20] . In

particular, an additional strength degradation of 10% is adopted for concrete during cooling down to ambient temperature, as compared to the strength value at the maximum reached temperature. The strain at peak stress and thermal properties are not recovered. For steel reinforcement, the yield strength is recovered to its initial value during cooling as long as the temperature has not exceeded 600 °C [21] . The thermal properties are generally considered reversible.

In the simulation, an initial imperfection is introduced to account for various secondary effects. It is assumed to be a single sine curve with a mid-height maximum deflection of L/1000 [22] [23] . The eccentricity e_0 is applied in the direction opposite to the imperfection to have the effects of eccentricity and imperfection adding up for bending in the same direction. The same imperfection (shape, relative magnitude, direction) is used for all the columns. The stirrups are not included in the numerical model since it is based on beam finite elements, and the members considered here are not subjected to shear failure. The load N is applied on top of the column within the first 20 s of the simulation and then maintained constant until failure, i.e. until the software is unable to find equilibrium for the structure. At that moment, an asymptote can be observed in the vertical displacement-time plot for the top node of the column, which indicates a ‘physical’ failure. Thus, in this numerical analysis, failure is defined as loss of structural integrity of the column, with no prescriptive failure criteria being applied. It captures both section failure and buckling failure.

4.3 Burnout Resistance Analysis

The natural fire selected for the burnout analysis is the fire model proposed in Chapter 2. For each test, the objective is to find the shortest 'standardized natural fire' that leads to failure under the considered applied load. Given the definition of the 'standardized natural fire' adopted above, the objective is to find the parameter DHP associated with each column (for the considered loading level). This parameter correlates to the ability to survive a fire until full burnout; it divides the time domain between fires that are short enough to be survived and fires that will result in eventual collapse (for the considered column, fire model, and load level). Finding the DHP of a column requires an iterative process, where a half interval search method is applied. As a result, several thermo-mechanical simulations are required for each of the 74 columns of Table 1 and each of the cooling rates K. The iterative process is shown in Chapter 3.

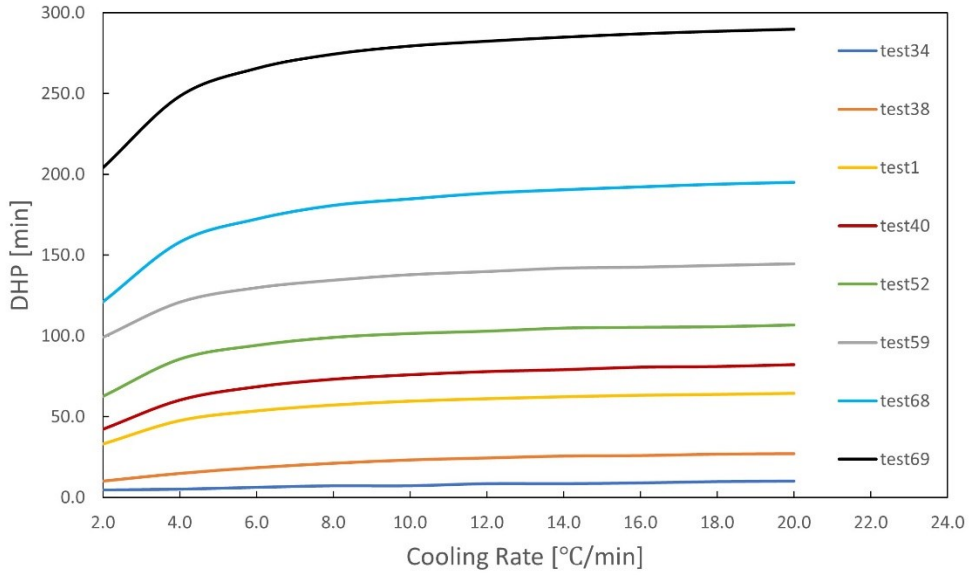

Figure 4-2 - DHP- Cooling Rate (K) for RC columns

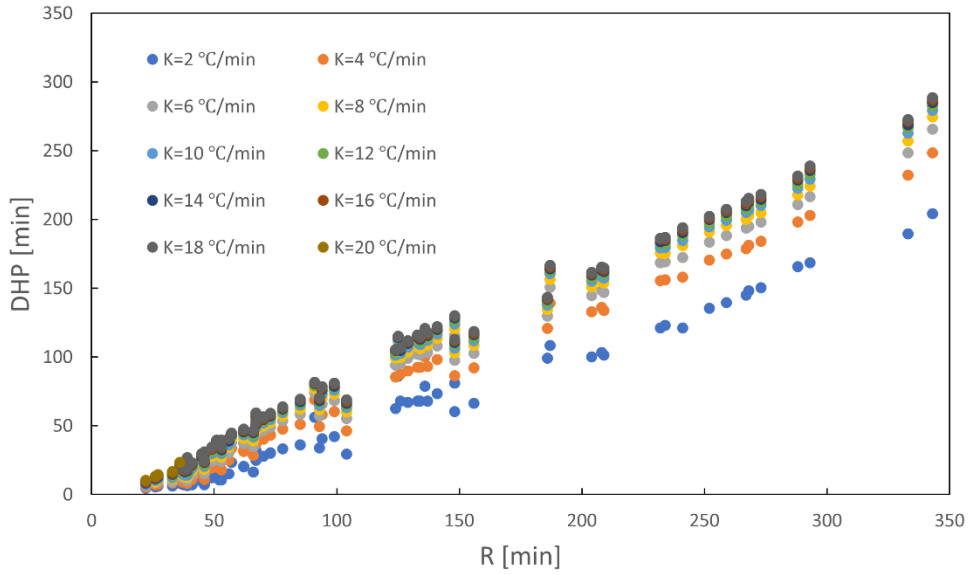

Figure 4-3 - DHP- Fire Resistance (R) relationship for RC columns

The computed fire burnout resistance, DHP, is given in Table 4-3. The DHP (or fire burnout resistance) is the shortest duration of the heating phase of the natural fire model leading to failure of the column, determined according to the flowchart of Figure 3-1. Values are given for ten values of the cooling rate K ranging from 2-20 °C/min. Figure 4-2 plots the relationship between DHP and K as computed numerically with SAFIR for the several test columns and figure 4-3 plots the relationship between DHP and R. From Table 4-3, it is clear that DHP is always shorter than R for a given column, which results from the definition of DHP (and the fact that, physically, the load-bearing capacity of any member continues to decrease during the cooling phase). From figure 4-2, the magnitude of DHP can be greatly influenced by the cooling rate, especially when the applied fire has a slow cooling phase. That is because the slow cooling phase makes the compartment to have a high gas temperature for a long time, which allows the cross section to absorb more heat after the heating phase and reach the maximum temperature much later. DHP is also observed to generally have a logarithmic relationship with cooling rate K. From figure 4-

3, DHP has a linear relationship with R and the slope of DHP and R would slightly increase when K increases. Such linear relationship is also observed by Gernay [5] when analyzing DHP of RC columns under the Eurocode parametric natural fire model.

The value of (R – DHP) can be used to measure the propensity to fail during or after the cooling phase for columns. The increase in (R – DHP) indicates a higher propensity to fail during or after the cooling phase. Figure 4-4 and 4-5 plot the relationship between R, K and (R-DHP) of several tests. (R-DHP) is also observed to generally have a logarithmic relationship with cooling rate K and an approximately linear relationship with R. It can be seen that (R-DHP) can be as much as 150 min in certain cases. Such great discrepancy indicates a high propensity for a concrete column to collapse during the cooling phase. Extra protections should be taken if the column is possible to be exposed to such natural fire.

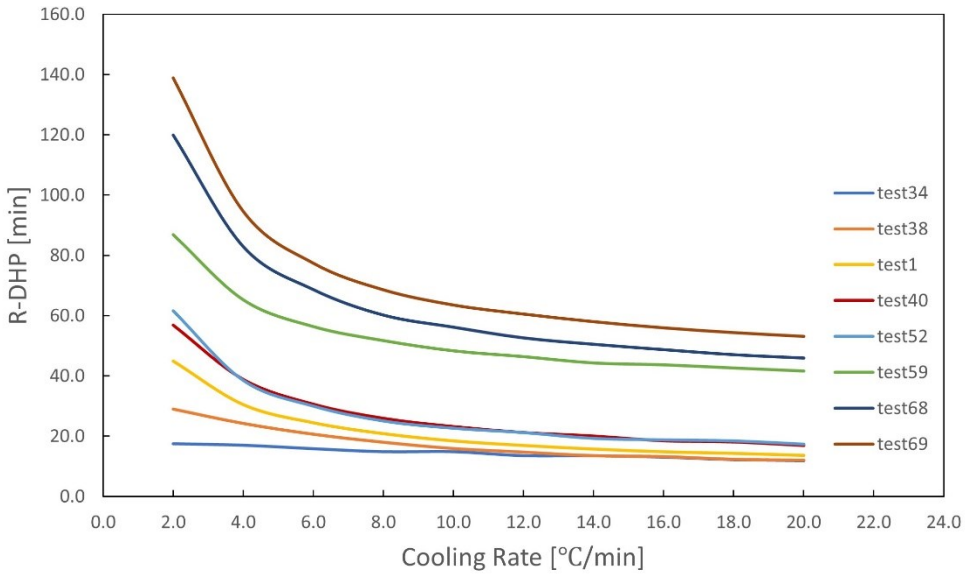

Figure 4-4 - (R-DHP)-R relationship for RC columns

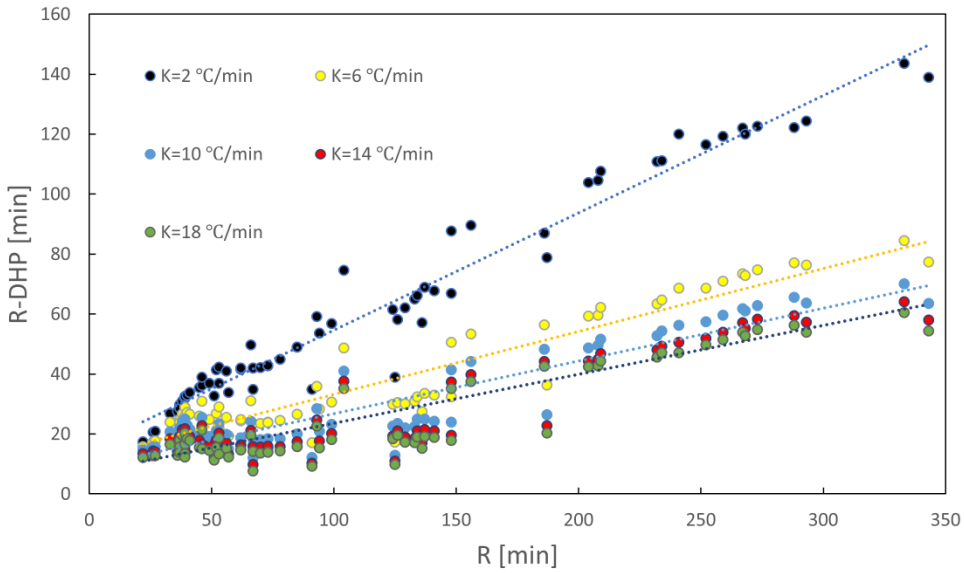

Figure 4-5 – (R-DHP)-K relationship for RC columns

Table 4-3 - Numerical simulation DHP Results

#	R test	R safir	DHP [min] as a function of K (°C/min)									
	[min]	[min]	2	4	6	8	10	12	14	16	18	20
test1	86	78	33.1	47.5	53.5	57.1	59.6	61.1	62.3	63.2	63.7	64.4
test2	84	85	36.1	51.0	58.4	62.3	65.0	66.3	67.6	68.9	69.2	70.2
test3	138	85	36.1	51.0	58.4	62.3	65.0	66.3	67.6	68.9	69.2	70.2
test4	63	62	20.5	32.2	37.6	41.0	43.4	44.8	45.6	46.7	47.2	48.6
test5	108	53	16.1	25.7	31.1	34.0	36.0	37.3	38.9	39.3	39.7	40.6
test6	61	49	12.1	19.1	24.1	27.5	29.9	31.4	32.9	33.3	34.5	34.8
test7	58	36	8.4	12.1	15.2	17.4	19.1	20.8	21.9	22.2	23.1	23.5
test8	58	37	7.5	10.1	13.3	15.0	16.8	18.2	19.1	20.2	20.5	21.4
test9	66	37	7.5	10.1	13.3	15.0	16.8	18.2	19.1	20.2	20.5	21.4
test10	48	33	6.1	8.2	9.0	11.2	12.2	13.5	14.6	15.4	16.5	16.7
test11	80	67	25.1	37.2	43.4	46.6	48.7	50.1	51.2	52.1	52.9	53.3
test12	69	67	25.1	37.2	43.4	46.6	48.7	50.1	51.2	52.1	52.9	53.3
test13	85	70	27.9	40.2	46.5	49.8	52.0	53.3	54.4	55.2	56.3	56.6
test14	49	37	7.5	9.1	12.1	13.8	15.0	16.8	17.9	18.2	19.1	19.5
test15	36	39	7.0	10.7	13.1	15.8	17.7	19.2	20.1	21.3	21.6	22.5
test16	75	62	20.0	31.5	37.2	41.0	43.4	44.8	45.7	46.7	47.4	48.6
test17	65	56	15.0	24.9	30.5	34.2	36.1	38.7	39.1	40.4	40.8	42.1
test18	49	41	7.2	11.1	14.4	16.9	19.4	20.6	21.9	22.4	23.1	24.4
test19	53	40	7.0	10.4	12.8	15.2	17.0	18.9	20.1	21.3	21.6	22.5
test20	111	141	73.3	98.3	108.1	113.5	116.7	118.9	120.0	121.4	122.2	123.3
test21	125	129	67.0	90.0	99.0	103.5	107.0	110.0	110.0	111.0	111.8	114.0
test22	40	38	7.1	9.2	11.3	13.0	14.1	16.0	16.6	17.5	18.4	18.7

test23	160	134	67.8	92.3	101.6	106.1	109.1	111.1	112.9	114.0	115.0	115.4
test24	89	136	78.8	100.1	108.6	113.4	115.8	117.6	118.9	120.0	120.8	121.3
test25	93	73	30.2	43.1	49.0	52.3	54.6	56.5	57.6	58.1	59.0	59.9
test26	135	73	30.1	43.3	49.2	52.3	54.6	56.1	57.1	58.2	59.1	59.3
test27	48	52	10.6	19.1	25.2	28.4	30.9	33.3	34.0	35.3	36.6	36.6
test28	57	66	16.2	28.4	34.9	39.1	41.8	43.2	44.9	45.9	46.4	47.2
test29	38	39	7.1	10.1	13.0	16.0	18.4	19.6	20.8	22.0	22.5	23.2
test30	55	53	10.8	18.0	24.0	27.3	29.6	31.3	32.7	34.0	34.4	35.6
test31	57	46	9.9	16.5	20.8	24.1	26.6	28.0	29.5	30.0	30.9	31.3
test32	49	37	7.3	10.1	13.2	15.5	17.4	19.0	20.0	20.8	21.3	22.2
test33	50	45	9.6	15.1	19.1	22.0	24.4	26.1	27.2	28.9	29.6	29.9
test34	31	22	4.6	5.1	6.2	7.2	7.2	8.5	8.5	9.0	9.8	10.2
test35	40	27	6.1	7.3	9.3	10.6	11.2	12.2	12.9	13.8	14.2	14.4
test36	35	26	5.5	7.0	8.6	9.2	10.2	11.7	11.7	12.1	13.3	13.3
test37	49	39	10.1	14.1	17.7	20.0	22.0	23.2	24.3	24.8	25.5	25.8
test38	52	39	10.1	14.8	18.4	21.1	23.2	24.3	25.5	25.8	26.7	27.0
test39	72	51	18.3	27.9	32.7	35.0	36.6	37.9	39.0	39.0	39.7	40.6
test40	61	99	42.2	60.2	68.4	73.0	75.8	77.7	78.9	80.5	80.9	82.0
test41	120	137	68.0	93.1	103.4	108.8	112.1	114.0	115.6	116.7	117.8	118.7
test42	125	125	86.1	102.1	107.8	111.2	112.1	113.7	114.1	115.2	115.2	115.7
test43	128	67	32.1	44.7	50.7	53.4	55.0	56.0	57.1	57.9	59.3	59.3
test44	116	148	81.1	106.1	115.6	120.6	124.0	126.1	128.5	129.7	130.1	131.2
test45	123	126	67.9	87.6	95.5	99.5	102.5	104.5	105.0	106.4	106.4	106.9
test46	126	91	56.2	69.0	73.8	76.7	78.9	79.5	80.7	81.0	81.8	82.1
test47	93	133	68.0	92.3	102.0	107.3	110.5	112.6	114.4	115.5	115.9	116.5
test48	60	37	8.4	12.9	16.3	18.6	20.1	21.1	22.2	23.1	23.1	23.6
test49	120	57	23.2	33.5	37.6	40.4	42.1	42.9	43.8	44.3	44.7	45.5
test50	60	46	7.0	11.1	15.1	18.1	20.4	21.8	23.2	23.9	24.6	25.1
test51	120	39	6.5	8.0	10.1	12.5	14.1	16.0	17.2	18.4	18.7	19.0
test52	63	124	62.5	85.5	94.1	99.0	101.4	102.8	104.7	105.2	105.6	106.7
test53	123	187	108.3	139.1	150.8	156.6	160.6	162.6	164.2	165.5	166.7	167.8
test54	107	94	40.4	58.0	65.7	70.1	73.1	75.6	76.3	77.5	78.6	78.9
test55	97	93	33.8	49.6	57.1	61.5	64.6	66.8	68.3	69.7	70.3	71.2
test56	170	192	100.1	132.8	144.8	151.1	155.3	157.3	159.8	160.5	161.6	162.8
test57	218	251	148.1	181.4	195.1	203.0	206.9	209.8	212.8	213.6	215.2	216.7
test58	220	269	165.8	198.1	210.9	218.0	222.5	225.7	228.5	230.0	231.7	232.7
test59	180	172	99.1	120.8	129.7	134.3	137.7	139.7	141.8	142.4	143.4	144.5
test60	208	217	121.2	155.5	168.7	175.5	179.3	182.2	183.9	185.6	186.4	187.3
test61	146	148	66.5	92.2	102.6	108.4	111.9	114.2	116.2	117.4	118.5	118.9
test62	187	196	103.4	135.9	148.3	154.6	158.5	161.5	163.1	164.6	165.3	166.1
test63	201	242	139.7	174.9	188.1	195.7	199.5	202.2	205.1	206.0	207.5	208.9
test64	210	236	135.5	170.5	183.5	190.8	194.5	197.2	200.0	200.9	202.4	203.7
test65	227	249	144.9	178.8	193.6	200.1	205.2	207.7	209.9	211.6	213.0	213.9
test66	234	255	150.4	184.3	198.2	204.9	210.2	212.7	214.7	216.7	218.1	218.9
test67	252	275	168.6	202.8	216.7	224.2	229.3	232.8	235.8	237.3	239.0	240.4

test68	225	228	121.1	158.1	172.3	180.8	184.8	188.4	190.5	192.3	193.9	195.0
test69	262	323	204.1	248.4	265.6	274.4	279.5	282.5	285.0	287.0	288.6	289.9
test70	285	308	189.5	232.2	248.4	257.2	262.9	266.5	268.9	271.3	272.5	273.7
test71	242	220	122.9	156.0	169.3	175.1	179.6	182.1	184.8	185.6	186.9	188.2
test72	220	198	101.3	133.8	146.8	153.9	157.4	160.1	162.2	163.6	164.7	166.3
test73	181	99	29.4	46.3	55.3	59.9	63.0	64.9	66.3	67.7	68.8	69.4
test74	183	141	60.3	86.5	97.5	103.0	106.6	108.9	110.7	111.8	112.9	114.0

4.4 Result Analysis Based on Equivalent Fire Severity

This section applies several methods to quantify the fire severity between different fire exposures. A simple DHP calculation method is derived at the end of this section. Different fire curves cause column failure because they have the same fire severity. The concept of equivalent fire severity is used to relate the severity of an expected real fire to the standard test fire. This is a good way when designers want to compare published fire resistance ratings from standard tests with estimates of the severity of a real fire. This section will try to apply several methods to quantify the fire severity of different burnout fire models that cause failure in the column by analyzing their thermal profile with SAFIR.

4.4.1 Equal Area Method

Ingberg [24] first proposed to compare the area under time–temperature curves to measure equivalent fire severity. Two fires are considered to have equivalent severity if the areas under each curve are equal, above a certain reference temperature. Even though this has little theoretical significance because the units of area are not meaningful, the equal area concept is a useful method of comparing fires.

To verify the applicability of this method, 100 ℃, 150 ℃, 200 ℃, 250℃ are selected as reference temperature. For instance, a dataset of the results of 200 ℃ reference temperature

is compiled in Table 4-4 and the relationship between time-temperature area and cooling rates for all tests is plotted as below in Fig. 4-6:

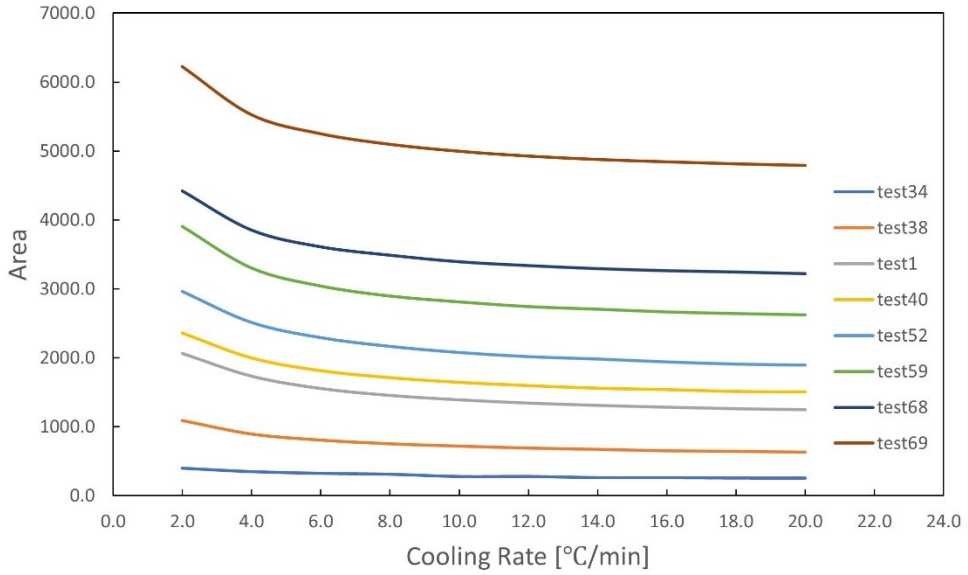

Figure 4-6 - Relationship between area and cooling rate

Table 4-4 - Area under time-temperature curves

#	Area									
	2.0	4.0	6.0	8.0	10.0	12.0	14.0	16.0	18.0	20.0
test1	2061.4	1731.2	1552.1	1451.8	1387.5	1340.4	1307.0	1280.4	1258.5	1243.9
test2	2163.2	1814.4	1647.1	1549.0	1481.0	1431.8	1399.9	1378.9	1354.5	1342.6
test3	2163.2	1814.4	1647.1	1549.0	1481.0	1431.8	1399.9	1378.9	1354.5	1342.6
test4	1591.5	1346.4	1201.7	1119.0	1071.1	1029.8	998.2	978.8	960.3	957.2
test5	1422.0	1183.5	1067.6	986.3	942.2	903.6	881.5	858.7	839.1	830.4
test6	1221.0	1015.6	916.0	858.4	816.7	789.2	770.0	747.3	737.4	724.4
test7	925.9	785.1	699.9	646.4	611.0	588.7	570.4	551.2	543.4	533.1
test8	821.3	697.1	633.4	584.3	551.7	535.3	517.5	507.1	492.5	489.6
test9	821.3	697.1	633.4	584.3	551.7	535.3	517.5	507.1	492.5	489.6
test10	695.4	589.0	511.4	486.3	456.1	440.7	430.2	420.8	417.5	406.0
test11	1777.1	1486.4	1338.2	1243.1	1183.6	1142.4	1112.1	1089.9	1071.0	1056.1
test12	1777.1	1486.4	1338.2	1243.1	1183.6	1142.4	1112.1	1089.9	1071.0	1056.1
test13	1858.7	1556.0	1405.3	1311.1	1252.7	1210.8	1176.7	1153.6	1138.9	1118.1
test14	821.3	678.3	629.8	575.2	545.6	528.2	514.4	499.2	492.6	482.4
test15	817.6	700.3	631.4	585.7	559.6	543.2	525.6	515.7	501.4	498.9
test16	1586.9	1332.0	1203.2	1124.9	1077.0	1035.7	1005.2	984.8	969.1	963.2
test17	1375.6	1160.0	1048.6	980.7	932.0	909.9	878.3	861.6	842.3	837.6

test18	818.9	720.5	643.0	593.9	572.9	545.9	528.7	512.1	503.2	502.9
test19	817.6	697.7	616.3	584.2	556.5	539.4	530.0	519.6	505.4	502.8
test20	3259.4	2781.6	2557.1	2432.8	2346.9	2289.0	2239.0	2208.5	2181.2	2166.4
test21	3094.8	2628.1	2398.4	2264.9	2187.8	2144.4	2085.4	2050.1	2023.1	2024.5
test22	817.9	677.6	607.2	560.6	536.7	527.1	503.5	494.7	488.6	477.4
test23	3105.0	2638.4	2413.3	2278.2	2194.7	2140.1	2104.2	2070.7	2047.5	2024.7
test24	3396.9	2854.1	2606.0	2474.2	2385.6	2323.1	2275.9	2242.7	2215.9	2193.5
test25	1958.7	1633.2	1465.2	1369.4	1304.5	1262.5	1229.2	1198.1	1180.6	1166.8
test26	1957.2	1635.8	1468.2	1370.2	1304.9	1259.0	1223.0	1199.3	1180.9	1159.9
test27	1095.4	962.2	878.6	812.6	771.6	755.5	726.9	713.5	704.2	687.2
test28	1422.9	1219.0	1103.2	1041.1	994.8	959.4	937.0	917.4	899.4	888.7
test29	817.9	695.5	629.6	592.7	565.0	537.7	523.3	513.8	503.5	497.6
test30	1097.1	952.5	870.0	811.2	768.4	741.9	721.6	708.3	693.2	690.7
test31	1019.8	895.1	799.7	747.9	713.2	684.8	667.9	646.7	635.2	624.0
test32	819.8	695.9	632.0	587.7	562.1	538.8	523.0	510.2	500.1	496.3
test33	1017.7	878.5	780.9	727.7	692.3	671.2	650.3	642.5	630.7	617.4
test34	395.1	345.3	320.7	307.5	274.9	275.7	258.7	258.8	253.6	251.3
test35	695.3	555.8	520.2	480.2	452.9	435.8	418.2	412.0	404.9	395.2
test36	555.1	501.3	442.8	407.1	384.8	374.2	350.5	341.9	342.3	330.9
test37	1091.5	888.7	793.0	737.0	699.6	674.6	655.7	636.0	626.2	612.3
test38	1091.5	895.7	807.7	753.6	720.1	691.4	672.7	651.7	643.4	632.0
test39	1509.2	1247.8	1121.0	1035.9	976.4	938.8	916.7	888.1	871.5	863.3
test40	2360.7	1999.0	1813.4	1712.8	1644.4	1596.9	1559.0	1538.9	1511.8	1504.5
test41	3122.2	2656.2	2441.1	2317.6	2238.0	2175.3	2136.1	2103.8	2081.3	2063.8
test42	3590.4	2991.7	2716.4	2569.3	2462.3	2397.4	2342.4	2308.7	2271.4	2249.7
test43	2026.8	1690.6	1524.1	1422.2	1349.7	1298.1	1263.6	1236.4	1228.0	1203.7
test44	3464.5	2949.7	2710.8	2571.1	2484.7	2424.0	2389.6	2357.6	2325.5	2307.1
test45	3105.8	2612.0	2373.2	2243.9	2163.2	2108.2	2056.9	2032.1	1995.2	1973.8
test46	2787.5	2300.5	2076.6	1947.1	1866.4	1803.0	1764.4	1725.7	1702.7	1682.4
test47	3122.2	2649.2	2426.9	2301.0	2220.9	2161.8	2125.4	2091.5	2061.2	2040.4
test48	925.9	792.7	713.1	658.7	622.1	591.8	572.4	558.1	540.6	531.0
test49	1704.2	1407.8	1245.7	1156.4	1099.1	1049.2	1019.5	992.7	972.9	964.4
test50	817.7	719.8	658.6	617.0	587.0	561.5	550.0	532.5	522.6	514.9
test51	698.2	588.4	533.7	505.3	485.4	475.6	461.3	454.0	439.7	428.8
test52	2962.5	2513.1	2293.0	2166.4	2077.6	2017.5	1982.8	1941.2	1909.1	1894.8
test53	4121.2	3538.0	3287.4	3144.8	3057.9	2990.0	2938.4	2902.9	2878.2	2860.6
test54	2298.7	1940.8	1762.1	1659.7	1593.0	1552.6	1507.5	1480.3	1461.6	1438.8
test55	2068.9	1747.2	1585.1	1491.4	1429.6	1386.5	1356.3	1336.4	1312.0	1297.4
test56	3931.0	3399.8	3153.9	3016.4	2930.5	2862.9	2824.1	2780.7	2754.2	2736.9
test57	5017.7	4355.1	4088.8	3950.3	3854.3	3791.5	3755.8	3708.9	3685.8	3669.8
test58	5397.8	4690.0	4405.1	4251.5	4153.7	4086.9	4047.7	4009.8	3988.7	3966.6
test59	3906.8	3303.3	3041.3	2896.3	2811.2	2743.0	2705.0	2665.3	2641.3	2622.5
test60	4419.4	3833.0	3581.1	3438.4	3347.8	3284.6	3236.5	3205.8	3173.2	3149.6
test61	3073.7	2621.7	2408.7	2288.8	2213.2	2155.5	2121.0	2088.1	2065.8	2040.0
test62	4005.3	3450.1	3205.7	3069.4	2980.5	2925.8	2878.8	2846.4	2812.8	2791.1

test63	4828.6	4192.4	3921.2	3778.4	3679.6	3613.5	3579.0	3531.5	3505.2	3488.8
test64	4737.8	4121.9	3850.5	3706.0	3606.3	3539.2	3503.6	3457.4	3434.8	3416.8
test65	4942.6	4290.7	4037.2	3879.3	3796.5	3727.6	3679.7	3644.0	3620.3	3596.1
test66	5066.6	4405.2	4141.5	3989.7	3907.4	3839.2	3788.0	3756.7	3730.3	3704.7
test67	5460.4	4750.1	4473.2	4325.7	4235.0	4173.4	4135.5	4097.0	4073.4	4055.1
test68	4417.3	3851.2	3609.0	3487.6	3393.1	3337.6	3293.5	3263.4	3244.4	3220.0
test69	6222.0	5526.1	5250.5	5097.7	4997.5	4927.6	4878.8	4844.4	4815.3	4792.6
test70	5909.0	5227.2	4956.9	4812.4	4723.3	4661.3	4610.6	4583.9	4553.5	4530.0
test71	4451.5	3856.2	3603.5	3448.3	3360.2	3296.3	3260.7	3218.3	3194.9	3180.5
test72	3957.3	3423.6	3187.5	3062.0	2968.1	2907.8	2868.9	2834.1	2807.9	2797.7
test73	1924.9	1648.4	1506.8	1418.4	1362.8	1320.5	1289.8	1269.0	1251.9	1234.8
test74	2904.2	2493.8	2290.1	2169.7	2095.1	2039.7	2003.2	1970.4	1948.0	1934.9

From Fig. 4-6, we can observe that, in all the tests, fire models with a low cooling rate have a larger area than fire models with a high cooling rate. The magnitude of the reference temperature (i.e. threshold to calculate the area) does not have an influence on such trend; similar results are obtained with the different tested thresholds. It is probably because heat transfer from a fire to the surface of a structure is mostly by radiation, the balance by convection. Since radiative heat transfer is proportional to the fourth power of the absolute temperature, heat transfer to the surface in a short hot fire may be much greater than in a long cool fire.

4.4.2 Maximum Temperature Method

A more realistic concept, developed by Law [25] and Lane [26] , is to define the equivalent fire severity as the time of exposure to the standard fire that would result in the same maximum temperature in a protected steel member as would occur in a complete burnout of the fire compartment. This method is also usually applied to evaluate time equivalency for RC beams by using rebar temperatures. For RC columns, since the rebar strength usually experiences larger degradation in high temperature than concrete, this research will

select the maximum corner rebar center temperature of the column before failure to compare different fires for simplicity. The maximum rebar center temperature is taken from the thermal analysis result of SAFIR. Figure 4-8 shows the temperature development of the rebar center of test 1 under different fire curves. To save computation time and cover a large enough fire resistance range, the maximum corner rebar temperature under different cooling rates of test 1,16,19, 21, 25, 27, 34, 40, 44, 46, 53, 63, 65, 67, 69 was plotted in figure 4-9. A dataset of the temperature results of the mentioned tests is compiled in Table 4-9.

From figure 4-8, we can observe that, for test1, the maximum rebar temperature is around the maximum rebar temperature of ISO834 fire test with a little variation, which confirms that this method is suitable for certain tests. However, from figure 4-9 and Table 4-5, for some tests, the maximum rebar temperature is quite different under different fire exposures. This is expected as, in general, the ultimate behavior of reinforced concrete columns is governed by other factors than the steel reinforcement alone. It can also be observed, from figure 4-10, 4-11 and 4-12, that the temperature distribution in the cross section at failure is different when the column is exposed to natural fire curves with different cooling rates. When the column is exposed a slow-cooling fire, the temperature distribution is more uniform. However, the temperature distribution at failure has more gradients under a fast-cooling fire especially around the rebar area. Unlike a RC beam, the concrete part of a RC column has a large influence on the strength of the member. When the compressive strength of rebars has a large influence on the compressive strength of column, this method of fire severity may be applicable. When the compressive strength of rebars is ignorable compared with that of concrete, this method is not applicable. In addition, it should be noticed that

the maximum rebar temperature is lower than 400 ℃ when the fire resistance is too low, which means the rebar strength is unchanged at failure. In these cases, this method does not work as well. Therefore, the maximum rebar temperature may work in some cases but, in general, it is not applicable to determine without a reinforced concrete column would survive a fire until full burnout or would eventually fail. Beyond the evaluation of the temperature distribution, this determination requires running a structural analysis as well.

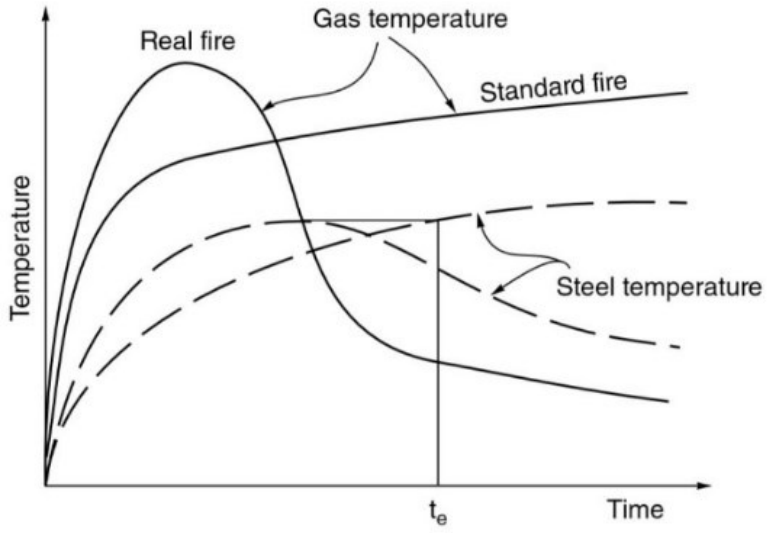

Figure 4-7 - Equivalent fire severity on temperature basis[27]

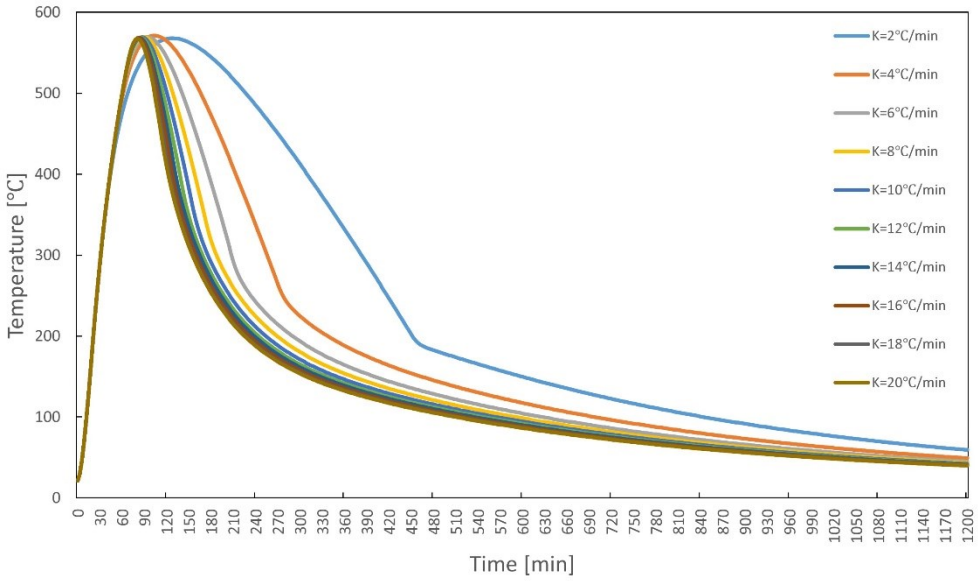

Figure 4-8 - temperature time relationship of rebar of test 1 under different cooling rates

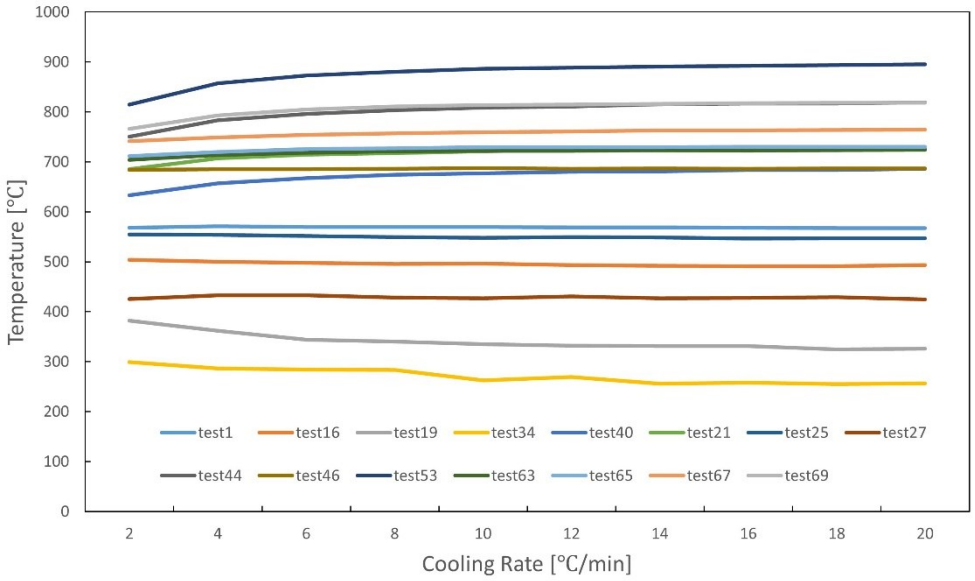

Figure 4-9 - Maximum rebar temperature under different cooling rates

Table 4-5 - Maximum rebar temperature

#	R	ISO834	Max. Rebar Temperature [°C]									
	min	[°C]	2	4	6	8	10	12	14	16	18	20
test1	78	571.4	567.8	571.2	569.5	569.5	569.2	568.9	568.5	568.2	567.1	567.4
test16	62	496.7	503.6	500.1	497.5	495.8	496.0	493.5	491.6	491.0	490.7	493.2
test19	40	332.4	374.9	360.9	343.8	340.4	335.2	332.0	331.5	330.9	324.8	325.6

test21	129	730.9	685.0	706.7	714.4	717.4	721.1	724.6	722.4	722.9	723.1	726.8
test25	73	542.4	554.6	553.8	551.6	549.1	548.1	549.0	548.2	546.5	547.0	547.3
test27	52	423.9	425.1	432.5	432.8	428.5	426.6	430.6	426.8	427.4	429.2	424.5
test34	22	277.74	299.0	286.5	284.0	283.1	262.8	268.9	255.4	258.3	255.0	256.6
test40	99	710.3	633.4	656.6	667.1	674.2	677.0	679.8	680.9	684.1	683.5	686.3
test44	148	837.9	750.0	783.4	796.1	803.0	808.3	811.2	815.2	816.9	817.0	818.9
test46	91	680.7	683.6	685.4	685.5	686.1	687.6	686.2	687.0	686.0	686.5	686.6
test53	187	915.2	814.4	856.8	872.7	880.5	886.1	888.3	890.4	892.2	893.9	895.3
test63	242	730.7	703.8	714.0	718.4	721.2	721.7	722.2	723.7	723.0	723.4	724.1
test65	249	735.2	711.7	719.9	725.9	727.3	729.2	729.2	729.6	729.8	730.2	730.1
test67	275	778.4	741.4	748.9	754.1	757.1	759.5	761.0	762.8	762.9	763.8	764.3
test69	323	833	766.3	793.2	804.8	810.5	813.4	814.7	816.0	817.2	818.0	818.6

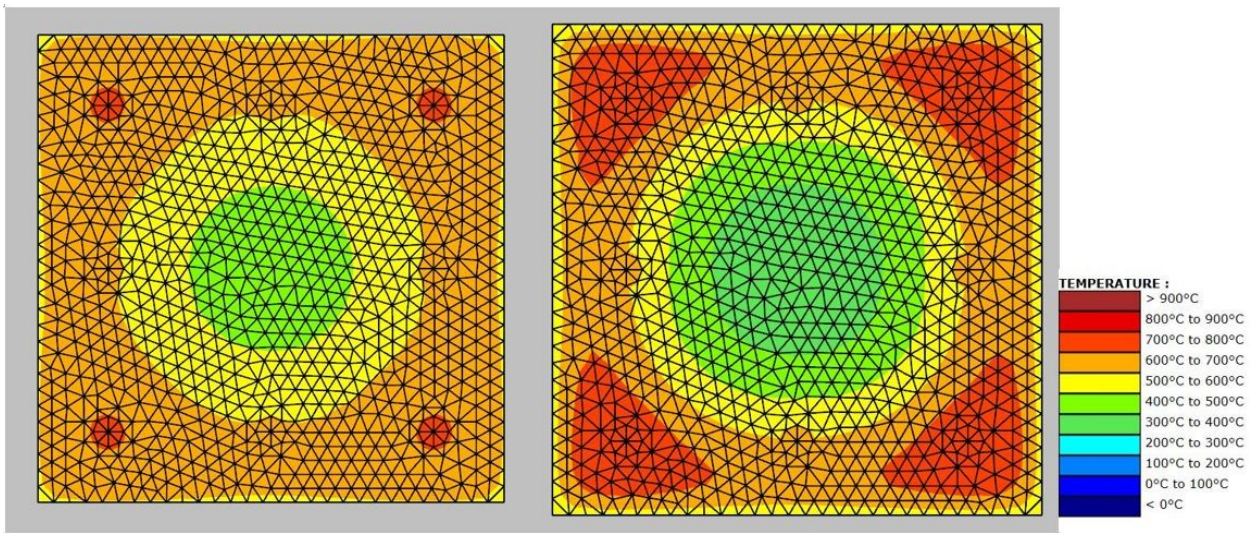

Figure 4-10 - Test 69 (R=323min) temperature distribution comparison at failure for different natural fires

(K=2 left, K=8 right)

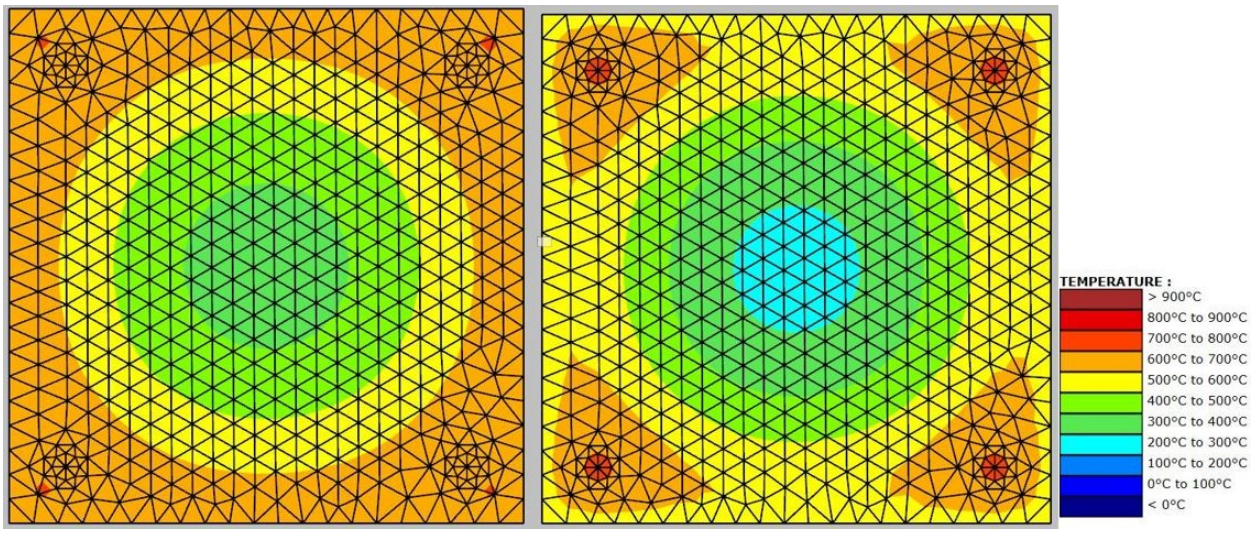

Figure 4-11 - Test 44 (R=148min) temperature distribution comparison at failure for different natural fires

(K=2 left, K=8 right)

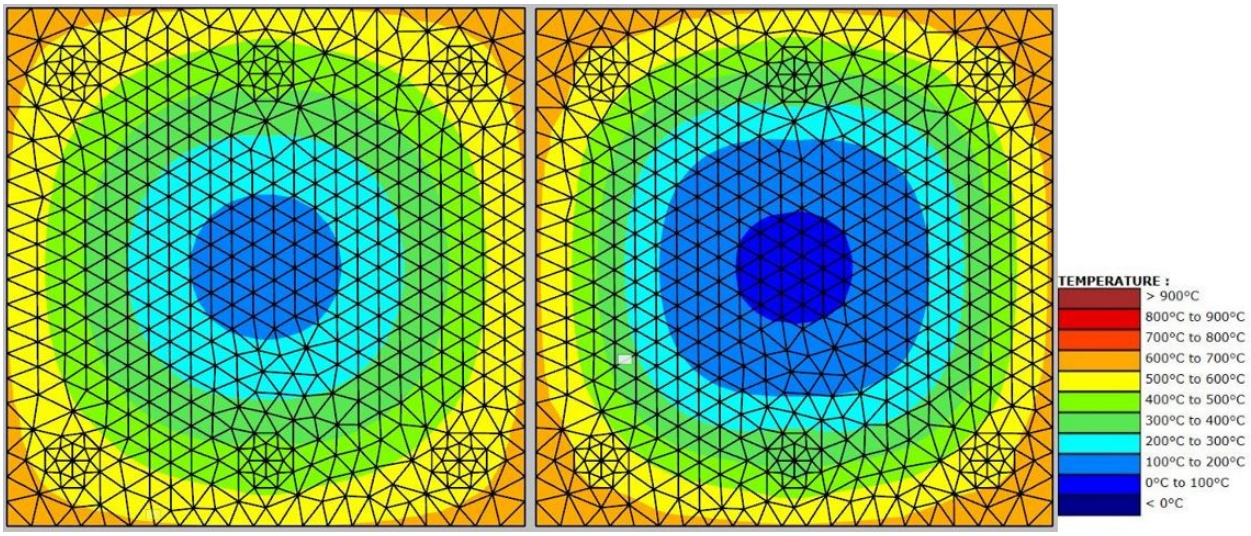

Figure 4-12 - Test 1 (R=78min) temperature distribution comparison at failure for different natural fires

(K=2 left, K=8 right)

4.4.3 Load Capacity Method

In a similar concept based on load capacity, the equivalent fire severity is the time of exposure to the standard fire that would result in the same load-bearing capacity as the minimum which would occur in a complete burnout of the fire cell. This concept is shown

in figure 4-10 where the load-bearing capacity of a structural member exposed to the standard fire decreases continuously, but the strength of the same member exposed to a real fire increases after the fire enters the decay period and the steel temperatures decrease. Although it would take longer computational time, this approach is a more realistic time equivalent concept for the design of load-bearing members.

This research will use the 500 °C isotherm method [19] to calculate the columns' load capability, in order to investigate whether a simple method of capacity evaluation could be used for burnout resistance analysis. In this research, the load capacity is based on the temperature distribution results of SAFIR thermal analysis. For the concrete part, when the temperature of one fiber is less than 500 ℃, the fiber retains its full strength. When the temperature is over 500 ℃, the fiber loses all its strength. Then, the area of fibers where temperature is less than 500 ℃ is added together and multiplies the compressive strength of concrete to calculate the load capacity. For the rebar, the strength of the rebar follows the strength-temperature relationship in Eurocode. Figure 4-14 shows the load capacity under different fire exposures of several tests and the data is compiled in Table 4-6. There is still some variation between the load capabilities at failure especially when the cooling rate is low. It is probably because the iso500therm method is not so accurate and the method applied here just simply calculates the compressive strength by adding every element together. It does not consider the influence of geometric imperfection, eccentricity, and slenderness ratio, which made the results different from the failure load evaluated by SAFIR. Therefore, the iso500therm method is not applicable either.

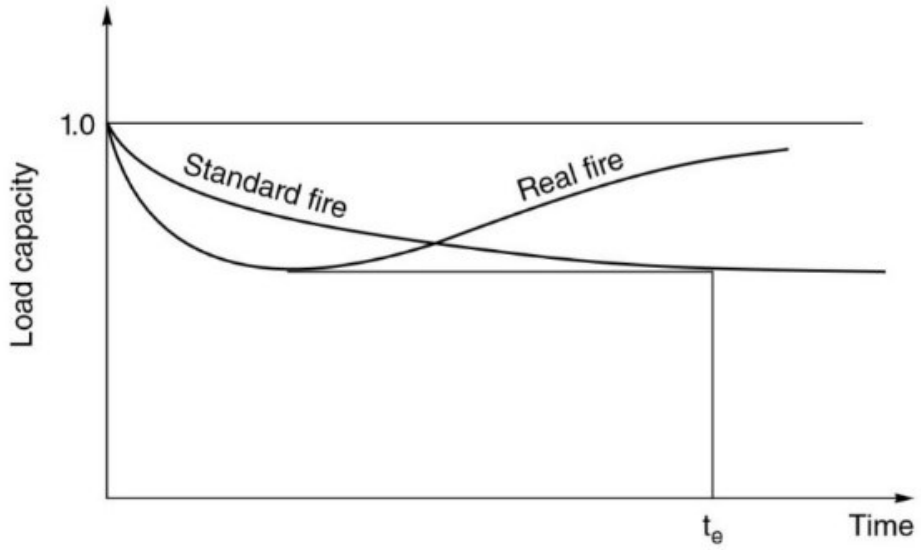

Figure 4-13 Equivalent fire severity on load capacity basis[27]

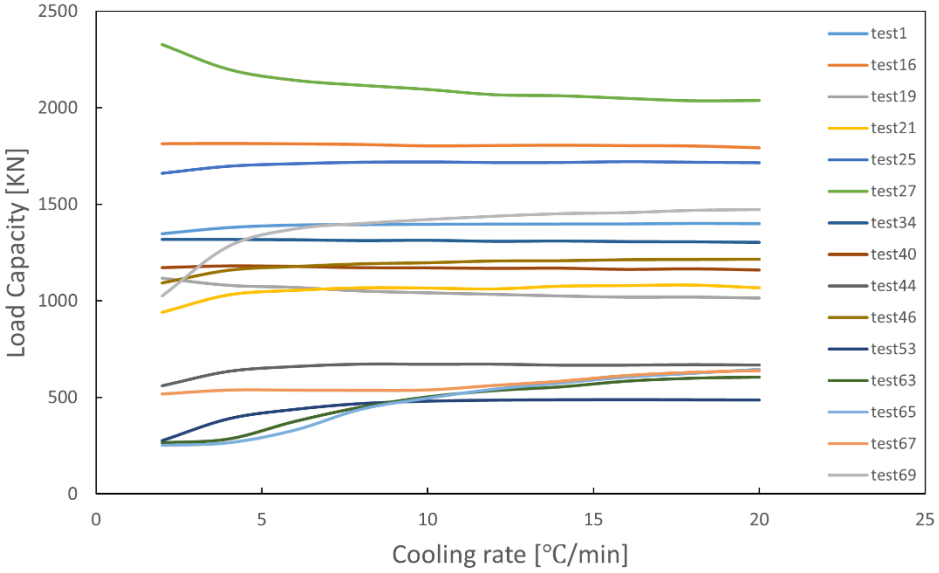

Figure 4-14 Load capacity under different cooling rates

Table 4-6 - Load Capacity at failure

#	R	ISO834	Load Capacity [kN]									
	min	[kN]	2	4	6	8	10	12	14	16	18	20
test1	78	1342	1347	1378	1391	1394	1395	1396	1396	1397	1400	1398
test16	62	1693	1812	1813	1812	1808	1801	1803	1805	1803	1801	1792
test19	40	919	1116	1080	1069	1051	1041	1034	1025	1019	1020	1014

test21	129	1060	939	1030	1054	1067	1066	1061	1076	1078	1081	1067
test25	73	1663	1660	1696	1709	1717	1719	1715	1716	1720	1717	1715
test27	52	1810	2326	2197	2141	2115	2093	2066	2060	2047	2034	2036
test34	22	1147	1318	1318	1316	1312	1314	1308	1310	1307	1306	1303
test40	99	1086	1171	1180	1177	1170	1170	1167	1168	1161	1164	1158
test44	148	631	559	633	658	671	670	670	665	665	668	666
test46	91	1220	1092	1159	1178	1192	1198	1207	1208	1214	1215	1216
test53	187	441	275	389	438	468	480	485	488	488	487	486
test63	242	458	265	285	376	450	503	536	555	585	600	605
test65	249	423	250	264	329	437	494	541	573	604	624	644
test67	275	574	517	538	537	536	538	562	584	613	630	638
test69	323	1390	1024	1282	1372	1400	1421	1438	1451	1457	1469	1473

4.5 A Data-based Equation for RC Column DHP Calculation

Based on the methods applied above, fire severity is a complex problem that cannot be explained by a single criterion. Gernay [5] has derived a simple equation that relates DHP to the standard fire resistance R computed by SAFIR, which is Eq. 4-1.

$$DHP = 0.72R-3 \tag{4-1}$$

However, the fire model used to derive this equation does not consider the influence of cooling rates. Therefore, an impact factor α that contemplates the influence of cooling rates is derived and added to Eq. 3 to refine it. From fig. 8, it can be observed that DHP can be greatly influenced by R and K. The relation between DHP and K can be fitted as a logarithmic function. Therefore, the impact factor α can be expressed as Eq. 4-2. Finally, the refined DHP equation is expressed as Eq. 4-3.

$$\alpha=\ln (f (R, K)) \tag{4-2}$$

$$DHP=\ln (f (R, K)) *(0.72R-3) \tag{4-3}$$

Based on the data of Table 4-3, the function f (R, K) can be fitted by a linear regression method. F (R, K) is given as Eq. 4-4. The refined DHP equation is given as Eq. 4-5.

$$F(R, K) = 0.84\sqrt[3]{K} - 26.32\frac{1}{R} + 1.49 \quad (4\text{-}4)$$

$$DHP = \ln\left(0.84\sqrt[3]{K} - 26.32\frac{1}{R} + 1.49\right) * (0.72R - 3) \quad (4\text{-}5)$$

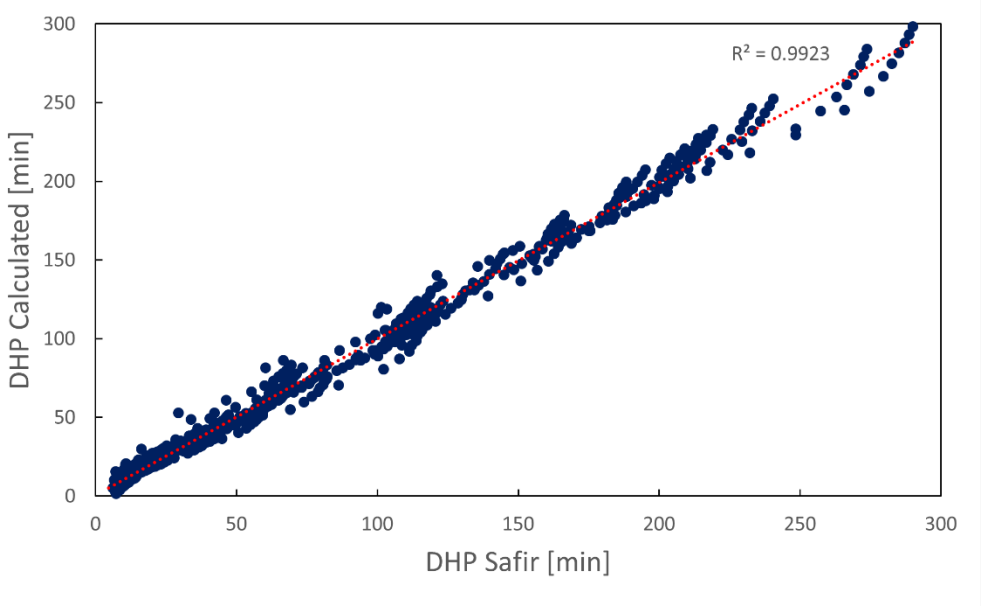

Figure 4-15 – Comparison between DHP predicted by Eq. 4-5 and DHP computed by Safir

Figure 4-15 compares the calculated DHP results with the results simulated by Safir. From this figure, we can see the DHP calculated by Eq.4-5 fits well with the simulated results with a R square value of 0.992. Therefore, this method is reasonable. This is remarkable since the computation of DHP requires a significant additional effort through application of the iterative process of figure 4-12. In contrast, Eq. 4-5 derives the DHP directly from R at no cost.

5. Burnout Resistance of RC Beams

5.1 Introduction

This chapter describes the numerical modeling and burnout resistance analysis of two RC beams under different fire exposures. The first beam is according to the standard fire resistance test conducted by Sauca [28] . It is used to compare numerical results with the test data to validate the ability of SAFIR to model RC beams under fire exposures. Figure 5-1 shows the general structure of the tested beam. The considered materials are concrete with the compressive strength of 48 MPa and cold worked steel, grade 500 class B. The beam is 8 meters in length and exposed to ISO 834 fire only between its supports. The beam is heated from three sides. The two cantilever parts of the beam are used to generate the support bending moment. The value of P is 18.4 kN and the value of P_{left} and P_{right} is 67.5 kN. Different reinforcements will be used at intermediate supports and the span as presented in figure 5-2.

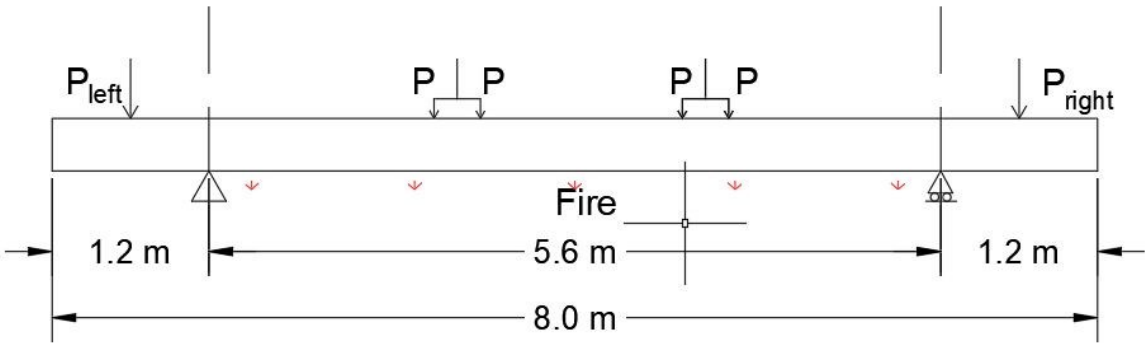

Figure 5-1 – Schematic representation of the structure of Ana's beam test

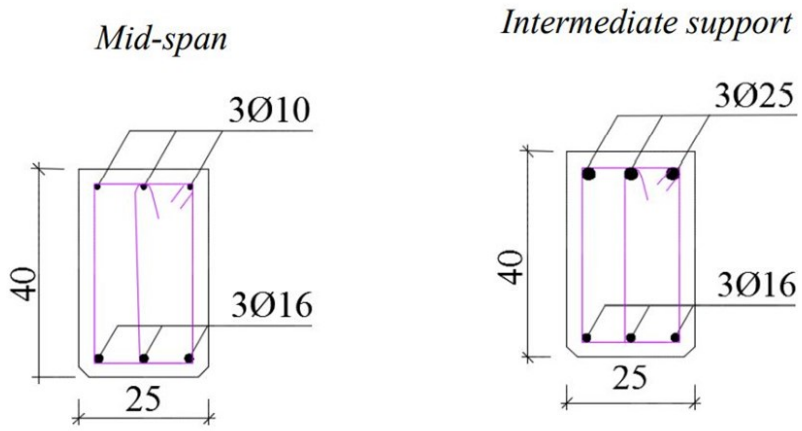

Figure 5-2 – Schematic representation of the cross sections [mm] of Ana's beam test[28]

After modeling the beam test, a typical RC beam used in buildings designed by V.K.R. Kodur and M. Dwaikat[29] is analyzed to trace its fire response in the entire range of loading up to collapse under fire exposure. According to ACI 216.1[30] , the fire resistance of this beam is calculated as 226 minutes[29] . This 6 m beam is exposed to a uniform load of 20 kN/m and heated from three sides along its span. The compressive strength of concrete is 30 MPa and the yield strength of reinforcements is 400 MPa. Details of the beam dimensions and load level are given in figure 5-3.

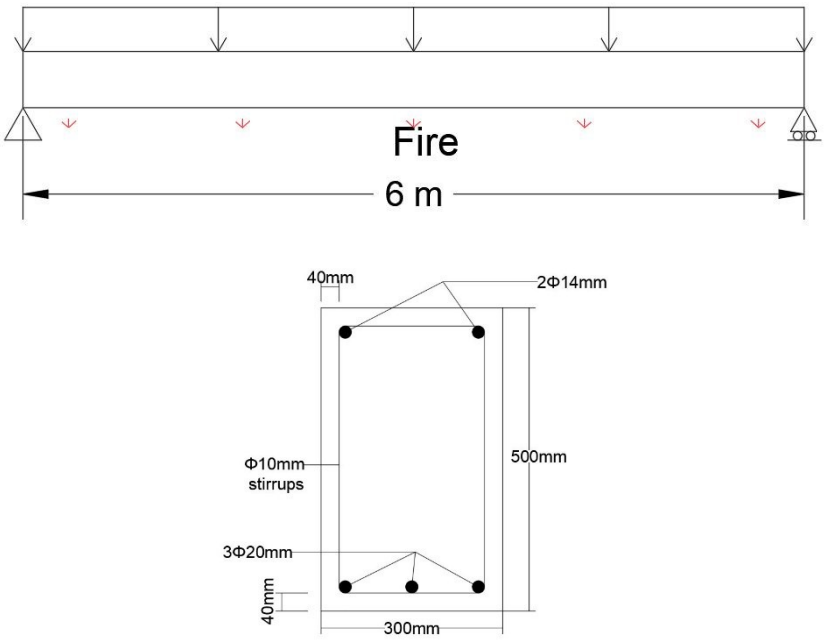

Figure 5-3 – Structure and cross section of the typical RC beam

5.2 Numerical Modeling and Verification

This section describes the numerical modeling process of the beams mentioned above. For simplicity, the beams are idealized as 2D structures. Both simulations use 2D conductive solid elements for thermal analysis and beam elements for structural analysis. Shear failure is not considered in this simulation since beam elements are selected for structural analysis.

Simulation of The Test RC Beam

The validity of the Safir model was established by comparing predicted results from the model with the measured values from fire tests for beams tested by Ana [28] .The structure is simulated as figure 5-1 and the cross section is simulated as figure 5-2. The aggregate type is silicious. Therefore, the concrete model is taken as 'SILCON_ETC' which adopts the explicit transient creep formulation [18] instead of the implicit formulation of the Eurocode. The equivalent cylinder strength f_{cm} is used for the concrete compressive

strength while a value of 1/10 of f_{cm} is assumed for the tensile strength. 'STEELEC2EN' is used for the reinforcement and the material is assumed as cold worked class B. The steel reinforcement yield strength is taken as f_{ym}. The material properties are summarized in Table 5-1. The convection coefficient on hot surfaces is taken as 25 W/m²K when modeling the thermal response under standard fire, as recommended in the Eurocode (while it is taken as 35 W/m²K under natural fire).

Table 5-1 - Summary of material properties for the test RC beam simulation

	Material Properties	Value
Concrete	Specific Mass [kg/m^3]	2359
	Moisture Content [kg/m^3]	72
	Convection Coeff. Hot [W/m^{2}K]	25
	Convection Coeff. Cold [W/m^{2}K]	4
	Relative Emission	0.7
	Parameter of Thermal Conductivity	0
	Poisson Ratio	0.2
	Compressive Strength [MPa]	48
	Tension Strength [MPa]	4.4
Steel	Convection Coeff. Hot [W/m^{2}K]	25
	Convection Coeff. Cold [W/m^{2}K]	4
	Relative Emission	0.7
	Young's Modulus [Gpa]	210
	Poisson Ratio	0.3
	Yield Strength [MPa]	500
	Type	Cold-worked class B

In the thermal analysis, the temperature distribution inside the cross-section is computed when the beam is exposed to fire. The cross section is discretized in the same way in Section 4.2. After the thermal analysis is finished, the predicted temperatures in SAFIR are compared with the measured temperatures in the test. Good agreement is observed between the two. Figure 5-4 presents the temperature evolution for both middle and corner rebars.

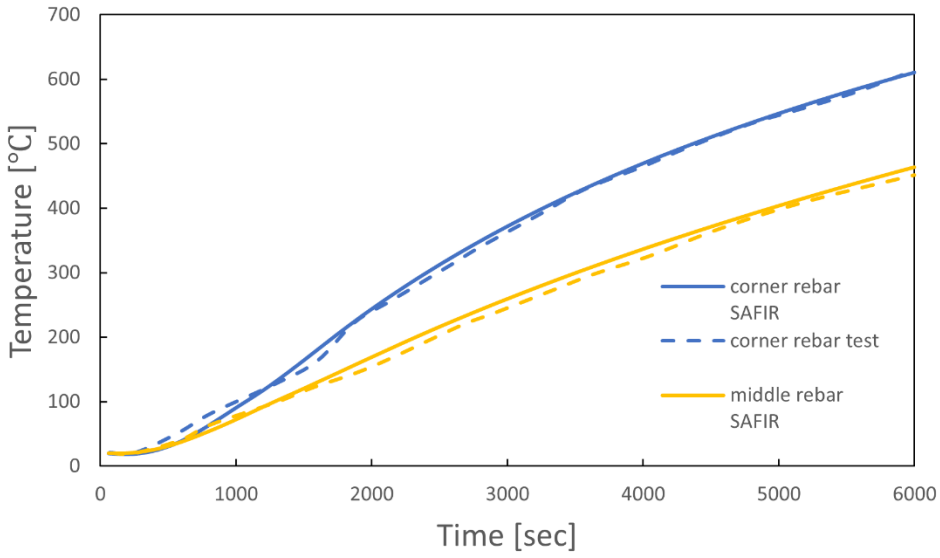

Figure 5-4 – Temperature evolution for both middle and corner rebars

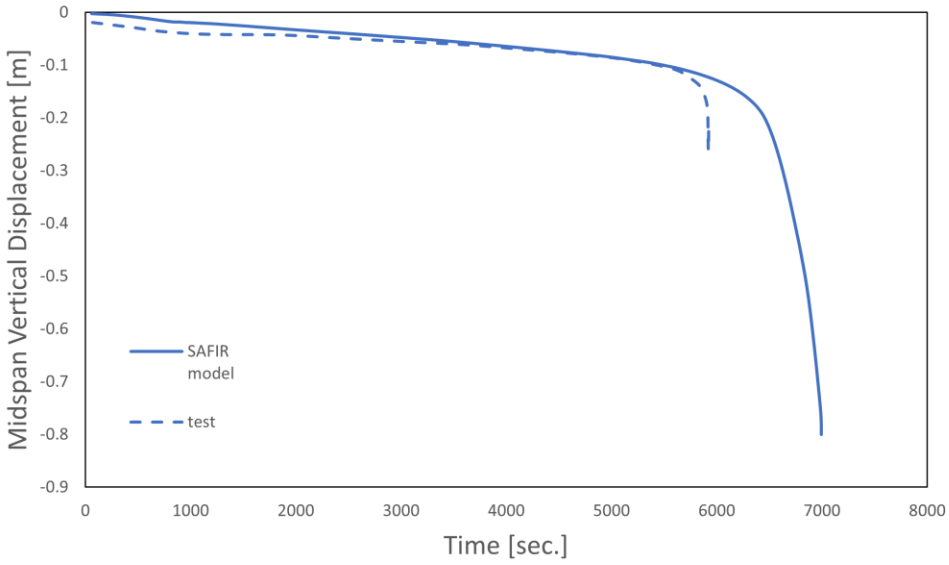

Figure 5-5 – Midspan vertical displacement evolution

In the test, the failure of the beam occurred at 99 min of fire exposure. The failure is due to the plastic hinge formed in the mid-span of the beam. Only one plastic hinge is formed since the standard tests are performed with simply supported boundary conditions. During the test, falling-off of concrete pieces occurred shortly before the failure time, as reported

by Sauca. This lead to a faster temperature increase in the rebars and an acceleration of the failure.

Numerical analysis performed in SAFIR predicted the failure to be reached after 115 min of fire exposure (the last step of convergence). The fire resistance computed by SAFIR is slightly larger than the test fire resistance because of the spalling of concrete during the test. Good agreement overall between the numerical solution and the test result is observed. Figure 5-5 compares the evolution of the mid-span vertical displacement measured during the test with the solution computed in SAFIR. The evolution of the measured mid-span displacement dur the test shows a similar trend with the mid-span displacement from the numerical analysis.

Simulation of The Typical RC Beam

The structure and the cross section are simulated as figure 5-2. Since the aggregate type is carbonate, 'CALCON_ETC' is used for the concrete model. The equivalent cylinder strength f_{cm} is used for the concrete compressive strength while a value of 1/10 of f_{cm} is assumed for the tensile strength. 'STEELEC2EN' is used for the reinforcement and the material is assumed as hot-roll class A. The steel reinforcement yield strength is taken as f_{ym}. The material properties are summarized in Table 5-2.

Table 5-2 - Summary of material properties for the typical RC beam simulation

	Material Properties	Value
Concrete	Specific Mass [kg/m^3]	2400
	Moisture Content [kg/m^3]	72
	Convection Coeff. Hot [W/m^{2}K]	25
	Convection Coeff. Cold [W/m^{2}K]	4
	Relative Emission	0.7
	Parameter of Thermal Conductivity	0

	Poisson Ratio	0.2
	Compressive Strength [MPa]	30
	Tension Strength [MPa]	3
Steel	Convection Coeff. Hot [W/m^{2}K]	25
	Convection Coeff. Cold [W/m^{2}K]	4
	Relative Emission	0.7
	Young's Modulus [Gpa]	210
	Poisson Ratio	0.3
	Yield Strength [MPa]	400
	Type	Hot-rolled class A

After the thermal analysis is finished, results from the analysis are used to demonstrate the behavior of a typical RC beam under fire conditions. To illustrate the thermal predictions from the model, the temperature variation is plotted as a function of fire exposure time at various locations of the beam cross section in figure 5-6. The temperature at various depths of concrete, as well as in rebars, increases with fire exposure time. As expected, the predicted temperature decreases with increasing distance from the fire exposed side. It can be seen that the unexposed side of the beam stays unaffected for the first 60 min of the fire exposure time. This is due to the low thermal conductivity and high thermal capacity of concrete which slows down heat penetration to the inner layers of concrete. Also, it can be seen in the figure that the temperatures in the corner rebar is higher than that for central rebar throughout fire exposure time. This trend is on expected lines and can be attributed to the fact that corner rebars are exposed to fire from two sides, while the central rebar is exposed to fire from the bottom face only. The steep increase in rebar temperature in the early stages of fire exposure is due to the occurrence of high thermal gradient at the beginning of fire exposure time as a result of faster increase in fire temperature.

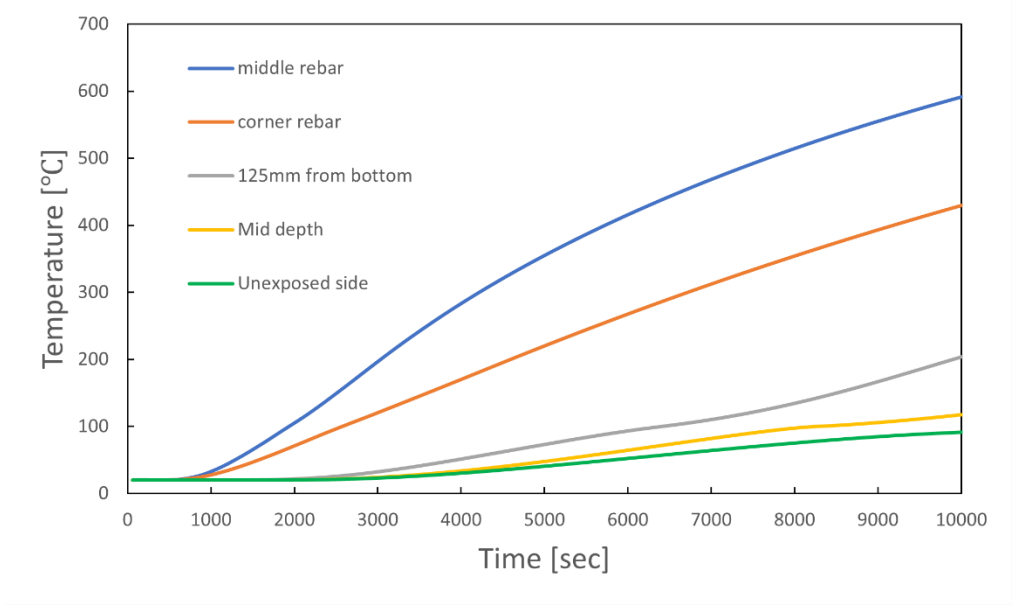

Figure 5-6 – Temperature evolution for the typical beam from SAFIR simulation

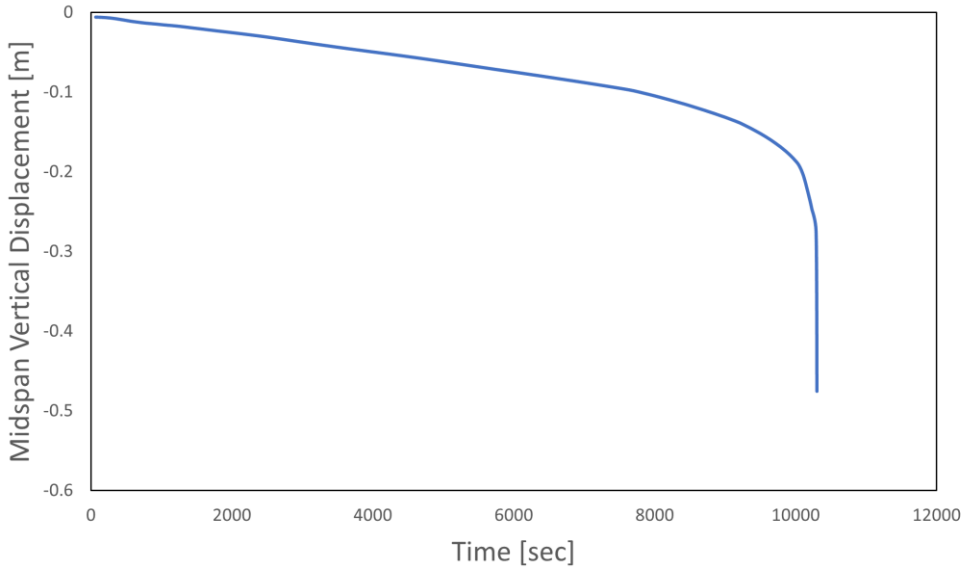

Figure 5-7 – Midspan vertical displacement evolution for the typical beam from SAFIR simulation

Numerical analysis performed in SAFIR predicted the failure to be reached around 180 min of fire exposure. Figure 5-7 shows the evolution of the mid-span vertical displacement until the structural collapse. The displacement of the beam shows a linear trend during the

initial stage of the fire due to the thermal loading. In addition, figure 5-7 also shows an increase in the beam deflection prior to failure. This trend is on the expected lines and is mainly due to the deterioration of material strength and stiffness and the yielding of steel. It can also be seen that the fire resistance for this beam, predicted by ACI 216.1, is higher than that predicted by SAFIR. This is probably because the prescriptive approach in ACI relates the fire resistance of RC beams to the concrete cover thickness and the width of the beam only and does not take into consideration factors such as load ratio and concrete strength[29] .

5.3 Burnout Resistance Analysis

The burnout resistances of these two beams are analyzed in this section. Several load conditions are applied on these beams to explore the relationship between traditional fire resistance, cooling phase and burnout resistance under different load conditions. These beams are analyzed under the proposed standardized natural fire model. The process of DHP calculation is generally the same as that of RC columns. Several thermo-mechanical simulations are iterated until finding the shortest ‘standardized natural fire’ that leads to failure under the applied load. The iterative method is described in Chapter 3 in detail.

The computed fire burnout resistance, DHP, is given in Table 5-3 and 5-4. The DHP (or burnout resistance) is defined as the shortest duration of the heating phase of the applied natural fire model leading to failure of the column, determined according to the flowchart of Figure 3-1. Figure 5-8 and 5-9 plot the relationship between R, K and DHP as computed numerically with SAFIR for the 10 beams. Beam 1 represents the beam tested by Sauca [28] and beam 2 represents the typical beam.

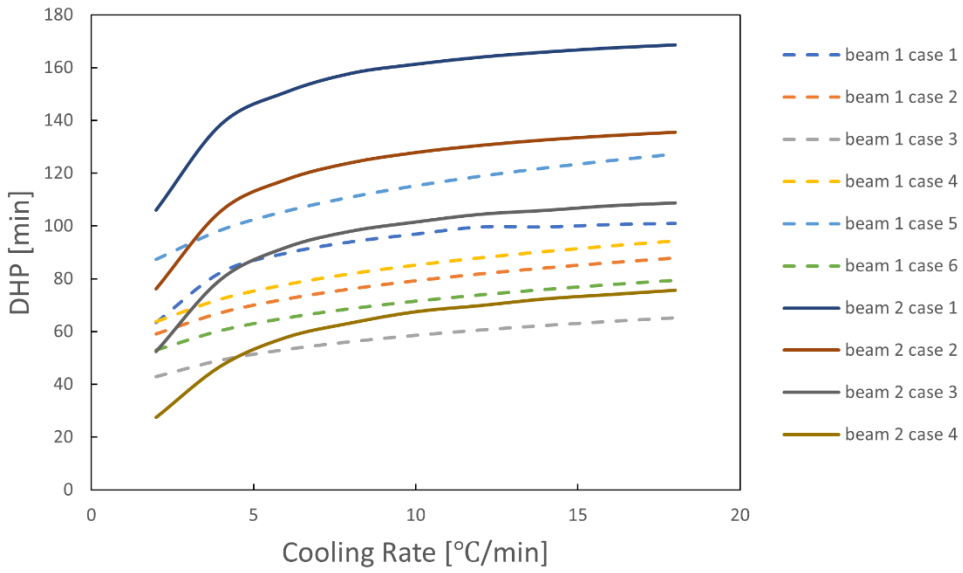

Figure 5-8 – DHP-K relationship for RC beams

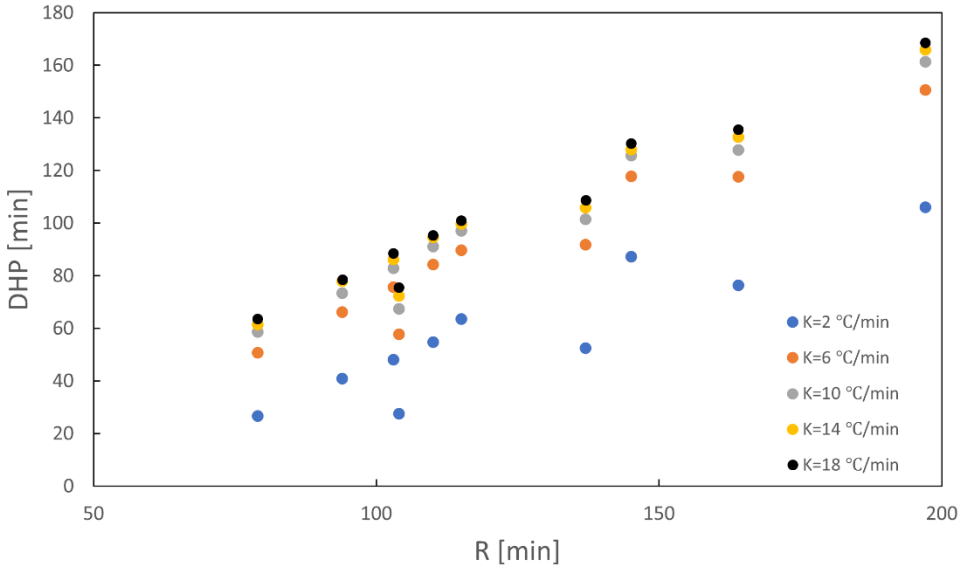

Figure 5-9 – DHP-R relationship for RC beams

The relationship between R, K and DHP of RC beams is quite similar to that of RC columns. The value of DHP can be easily observed to be always shorter than R for any given beam. DHP generally has a logarithmic relationship with cooling rate K and a linear relationship with R. It should be noted that the load condition might have an influence on the DHP

especially when K is small. The DHP of beam 2 which is uniformly loaded is much smaller when K equals 2 ℃/min than that of beam 1 which only has concentrated loads. The difference between the DHP and R is usually large when K is small or R is large.

Table 5-3 - Summary of DHP for the RC beam tested by Sauca

Case	P_{right}/ P_{left} [kN]	P [kN]	R [min]	DHP [min]								
				2 ℃/ min	4 ℃/ min	6 ℃/ min	8 ℃/ min	10 ℃/ min	12 ℃/ min	14 ℃/ min	16 ℃/ min	18 ℃/ min
1	67.5	18.4	115	63.4	82.5	89.7	94.0	97.0	99.7	99.7	100.6	101.0
2	97.5	25.4	103	48.1	67.2	75.6	80.1	82.9	85.3	86.1	86.9	88.5
3	136	36	79	26.5	43.2	50.6	55.5	58.6	60.5	61.4	63.0	63.6
4	0	95	110	54.8	75.2	84.2	88.5	91.1	92.4	94.5	94.5	95.4
5	0	75	145	87.2	109.9	117.7	122.1	125.7	126.6	128.0	129.0	130.3
6	0	120	94	40.8	58.0	66.1	72.0	73.3	75.6	77.8	77.8	78.6

Table 5-4 - Summary of DHP for the typical RC beam

Case	Uniform Load kN/m	R [min]	DHP [min]								
			2 ℃/ min	4 ℃/ min	6 ℃/ min	8 ℃/ min	10 ℃/ min	12 ℃/ min	14 ℃/ min	16 ℃/ min	18 ℃/ min
1	15	197	106.0	138.5	150.6	157.8	161.2	163.9	165.8	167.4	168.5
2	20	164	76.2	105.7	117.6	124.0	127.8	130.5	132.6	134.2	135.5
3	25	137	52.4	79.7	91.8	97.9	101.4	104.4	105.8	107.6	108.6
4	30	104	27.4	46.9	57.7	63.2	67.4	69.8	72.3	73.9	75.6

5.4 Result Analysis Based on Equivalent Fire Severity

In this chapter, RC beams are only considered for bending failure under various fire exposures due to the selection of beam elements. Bending failure is mostly caused by yielding of the steel reinforcements. In addition, the strength of reinforcement decreases when it is at a high temperature. In Eurocode, the effective yield strength of steel would drop to 47% when the temperature is over 600 ℃ and reduce to close to zero when the temperature exceeds 1000 ℃. Therefore, the maximum rebar temperature is considered to be one of the most important factors that lead to the bending failure of RC beams. The

maximum rebar temperature is selected here for equivalent fire severity analysis. This research will select the maximum temperature of the center of corner rebar before failure to compare different fires for simplicity. The maximum temperature can be taken from the thermal analysis result of Safir. Figure 5-10 shows the temperature development of the center of the corner rebar of beam 1 case 1 under different fire curves. The maximum corner rebar temperature under different cooling rates is plotted in figure 5-8. A dataset of the temperature results of the mentioned tests is compiled in Table 5-4.

From figure 5-10, we can observe that, the rebar temperature will still increase after the heating phase of the fire, which causes the structural delayed failure. The rebar temperature will increase in a slow and durable way for slow-cooling fires and a fast but short way for fast cooling fires, which corresponds to the characteristics of the applied fire. In figure 5-11, the maximum rebar temperature slightly increases when the cooling rate increases. It is because of heating transfer process of RC beams. We can also see that the maximum rebar temperature is basically at the same level even though the member is heated in different ways. In addition, compared with the maximum rebar temperature got from the ISO834 fire test, the maximum rebar temperatures got from different natural fire are still at the same level. It indicates the applicability of relating the maximum rebar temperature of natural fire tests to that of standard fire test. The maximum rebar temperature method is more suitable for RC beams than RC columns since the failure is mostly controlled by the strength of rebars under fire exposures. Figure 5-12 shows the cross-sectional temperature distribution at the time of failure for several natural fire exposures. The temperature distribution is much more similar than that of columns, which corresponds to their different

failure mode. Therefore, the maximum rebar temperature method seems applicable for RC beams.

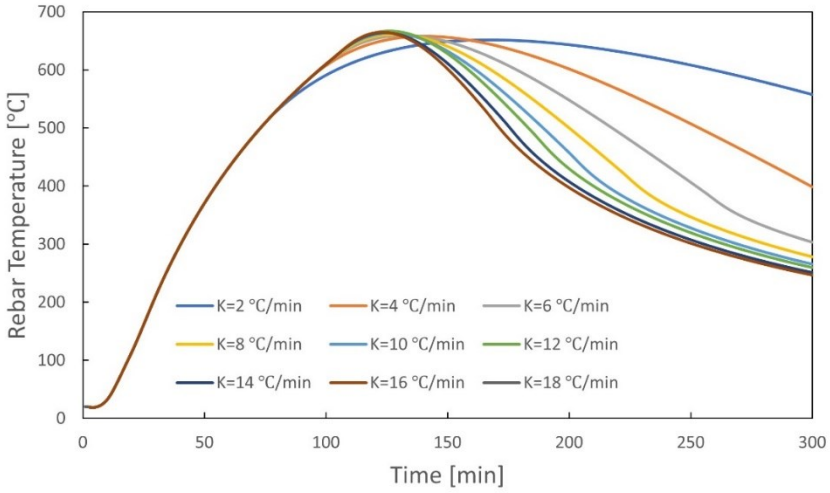

Figure 5-10 – Temperature development of rebar of beam1 case 1 under different cooling rates

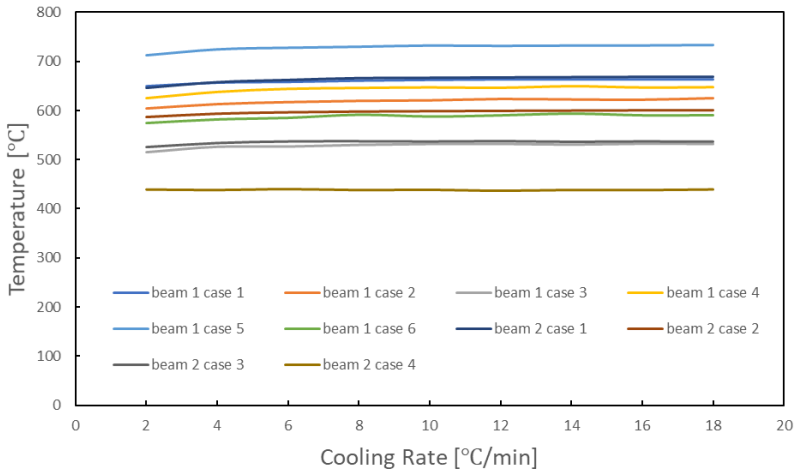

Figure 5-11 – Summary of maximum rebar temperature for RC beams under different cooling rates

Table 5-5 - Summary of maximum rebar temperature for RC beams under different cooling rates

#	R	Maximum rebar temperature [°C]									
	[min]	ISO 834	2 °C/min	4 °C/min	6 °C/min	8 °C/min	10 °C/min	12 °C/min	14 °C/min	16 °C/min	18 °C/min
beam1 case1	115	659.3	650.5	657.5	659.0	661.5	663.0	664.0	663.8	663.9	664.0
beam1 case2	103	620.8	603.5	612.6	616.8	619.3	620.4	623.4	622.3	621.8	625.0
beam1 case3	79	528.2	514.7	526.4	526.8	530.4	532.3	532.6	530.9	532.8	532.3
beam1 case4	110	643.8	624.4	637.1	643.4	645.3	646.5	645.7	648.8	646.3	646.9
beam1 case5	145	732.1	712.5	724.9	728.3	730.5	733.0	732.3	733.0	733.2	734.1
beam1 case6	94	588.9	575.3	582.5	585.6	591.7	588.2	590.5	593.9	590.7	590.8
beam2 case1	197	669.8	646.7	657.8	662.2	665.8	666.4	667.2	667.7	668.2	668.5
beam2 case2	164	601.1	586.1	593.2	596.2	597.8	598.6	599.3	599.9	600.4	600.7
beam2 case3	137	534.7	525.3	533.4	536.4	536.9	536.3	537.1	535.8	536.5	536.1
beam2 case4	104	435.8	439.7	438.8	440.4	438.7	439.2	437.4	439.0	438.7	439.8

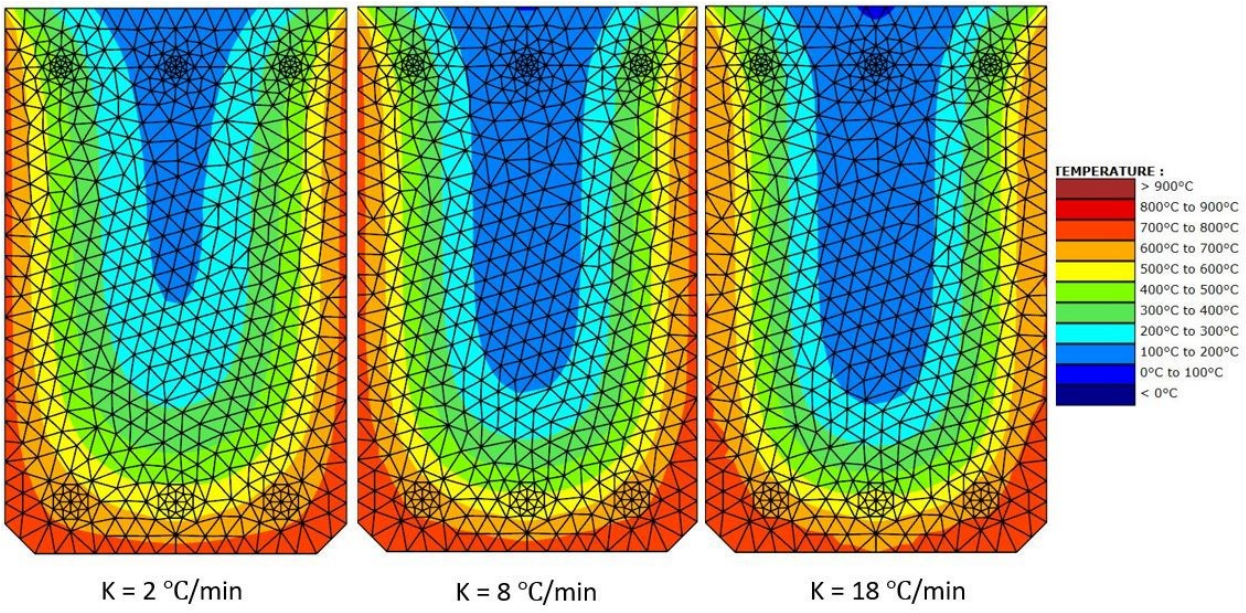

(a)

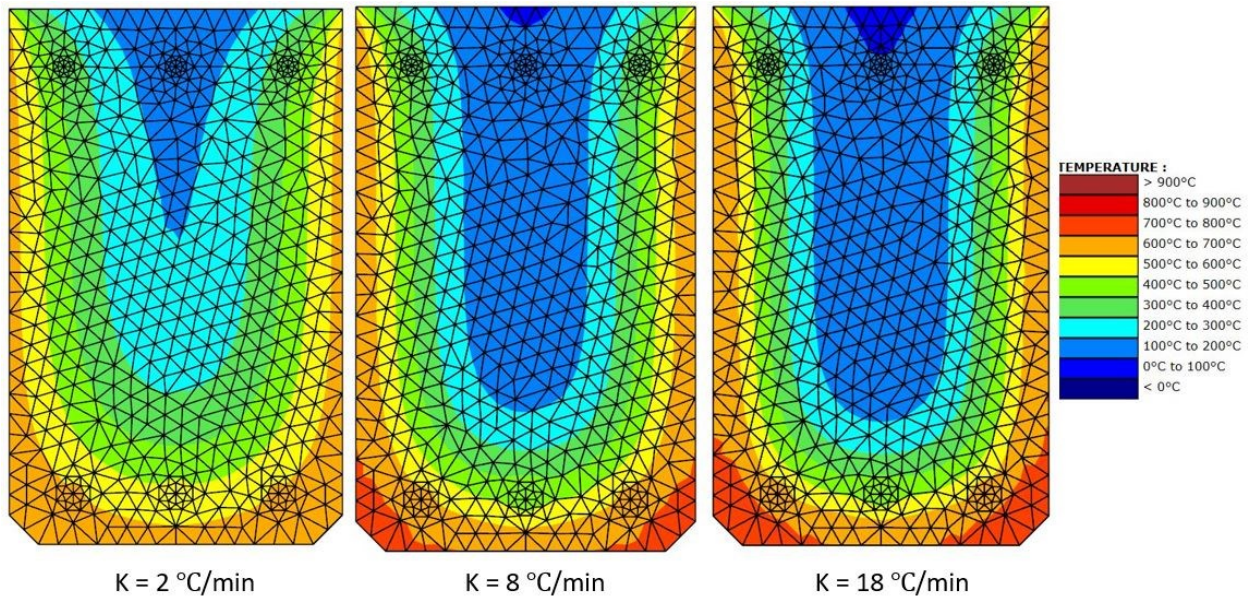

(b)

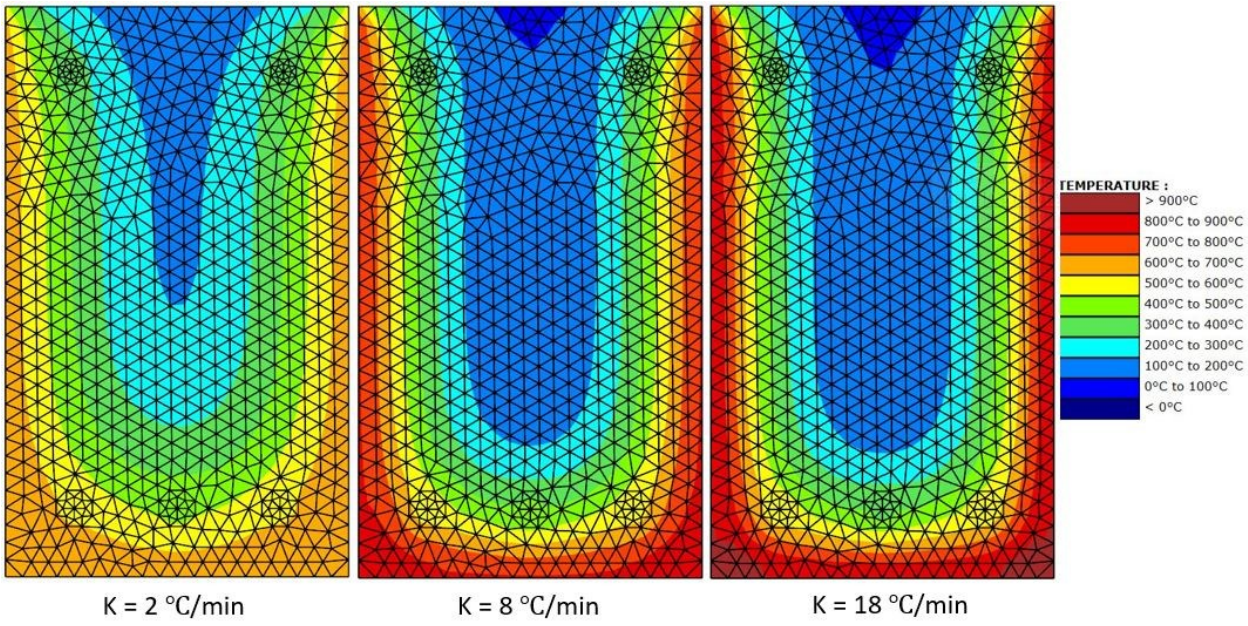

(c)

Figure 5-12 – Cross-sectional temperature distribution of different tests at failure for natural fire with K=2, K=8 and K=18 (a. beam 1 case 3, b. beam 1 case 2, c. beam 2 case 2)

5.5 A Data-based Equation for RC Beam DHP Caculation

This section aims at deriving an equation to relate DHP directly as a function of R and K. Eq. 4-5 proposed in Section 4.5 for RC columns is firstly applied to see if the equation for columns can predict the DHP of wall accurately.

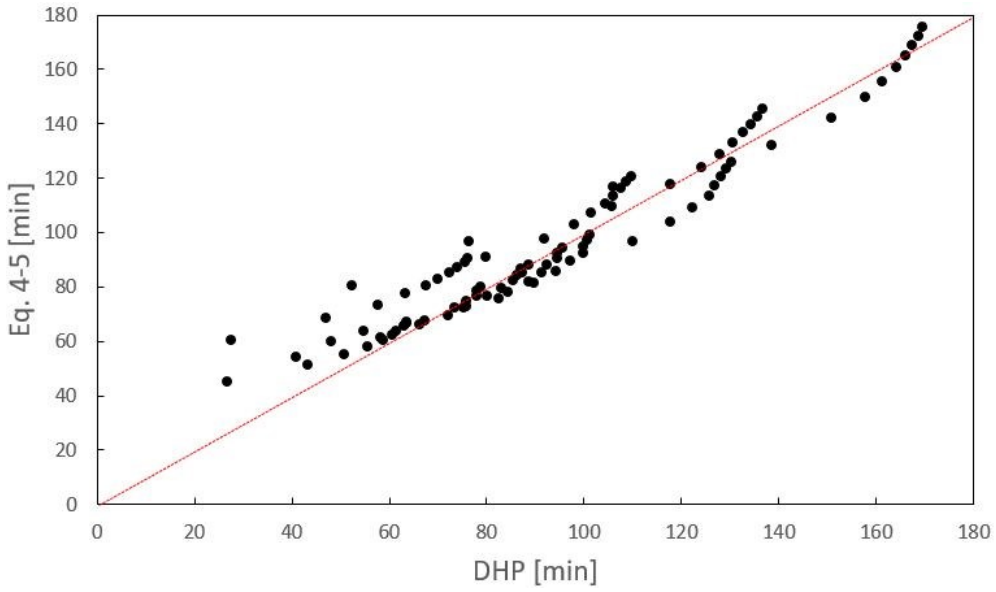

Figure 5-13 Comparison between DHP and the results calculated by Eq. 4-5

Figure 5-13 compares the results predicted by Eq. 4-5 with the real DHPs got from Safir. It can be seen that the agreement between the results predicted by Eq. 4-5 and the real DHP evaluated from SAFIR is reasonable with an R square value of 0.923. It shows that the relationship between R, K and DHP of RC beams is very similar to that of RC columns. Therefore, for simplicity, Eq. 4-5 is still able to roughly estimate the burnout resistance of RC beams. It is convenient for engineers to estimate the burnout resistance at the beginning, which will save a lot of computational time and effort. However, it should be noticed that, since the failure mode of beams is different from that of columns, the result of Eq. 4-5 is still not accurate enough. Further research is needed to calculate the burnout resistance of RC beams more accurately and efficiently. Alternatively, as shown above, the

determination of the peak temperature reached in the lower steel reinforcement (throughout the entire fire duration) provides a good estimation to determine whether a beam would survive to full burnout.

6. Burnout Resistance of RC Walls

6.1 Introduction

Figure 6-1 Details of the test RC wall (a. rebar layout, b. test setup)

In this chapter, the burnout resistance is analyzed for a high-rise RC wall tested by Pham et al. [31] in 2021. The test is designed to investigate the behavior of a slender wall with a very large height/thickness ratio under standard fire exposure. The tested wall is 2.6 m-wide, 8.4 m-high and 0.15 m-thick. The height/thickness ratio equals 56. It is heated by ISO 834 fire on one side for 90 minutes and only subjected to the thermal load and its self-weight. In terms of the boundary conditions, the wall is hinged at both ends and the top support can move vertically. The concrete has a compressive strength of 36.1 MPa and tensile strength of 2.75 MPa. For the reinforcements, the wall was reinforced by two

symmetrical layers of 9 mm diameter hot rolled steel reinforcing bars of yield stress fy = 480 Mpa and Young's modulus Es = 210 Gpa, with a spacing of 100 mm. The steel bars were arranged in two orthogonal arrays and placed with 25 mm of concrete cover at both the top and the bottom parts of the wall thickness. Figure 6-1 shows the details of reinforcements layout and the test setup. The experimental results show a large deflection of the high wall in fire conditions (almost equal to the wall height/24) for a fire exposure time of 90 min and emphasize the importance of high-rise walls protection under fire exposure.

A numerical model is firstly calibrated in SAFIR to reproduce the test result and verify the applicability of this numerical approach. Then, the load capacity of this structure at ambient temperature is calculated. The burnout analysis is conducted when different load is applied on this wall to explore the behavior of such high-rise wall under natural fire exposure. Finally, based on the numerical results, a data-based equation for the burnout resistance such high-rise wall is derived.

6.2 Numerical Modeling and Verification

This section describes the numerical modeling process of the test wall and verify the applicability of this numerical model. Then the load capacity of this model at ambient temperature (20 ℃) is calculated by SAFIR. The numerical model was verified by comparing predicted numerical solution with the measured test results. Shell elements were used for the structural analysis. In SAFIR, the shell element is a four-node quadrilateral element. It is defined by four corner nodes and a constant thickness, h. The center of the local coordinate system lies at the intersection between a-c and b-d. The z-axis is

perpendicular to the a–c and b-d plane. Figure 6-2 shows the geometry of a shell element in SAFIR in detail. There are four Gauss integration points on the surface of the shell element. There are also integration points distributed across the depth of the shell at the positions of the surface integration points. A transient uniaxial temperature field across the depth of the shell, obtained from the thermal analysis, is taken into account. The number of Gauss integration points across the thickness is defined by the user.

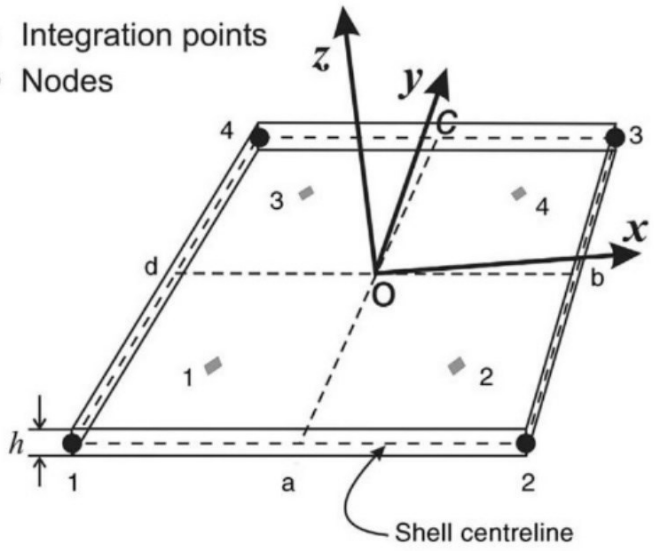

Figure 6-2 – Geometry of a shell element in Safir [32]

This type of element is usually used to model structures where one dimension, thickness, is significantly smaller than the other two dimensions. It is thus very suitable for structures such as walls and slabs. For instance, Lim [33] used shell elements to model two-way reinforced concrete slabs in fire in SAFIR. The numerical results showed good agreement with tests results and verified that the SAFIR shell element is useful in modeling structural behavior of reinforced concrete slabs in fire conditions.

To model this high-rise RC wall, the material properties are summarized in Table 6-1. The concrete model is taken as ‘SILCON_ETC’ for thermal analysis and ‘SILCOETC2D’ for

structural analysis. Both of them adopt the explicit transient creep formulation [18] instead of the implicit formulation of the Eurocode. SILCOETC2D is a temperature-dependent plastic-damage constitutive model described in Gernay et al.[34] . This constitutive model has been validated for simulating the behavior of reinforced concrete walls under one-side thermal exposure using shell elements in SAFIR[35] . 'STEELEC2EN' is used for the reinforcement and the material is assumed as hot-rolled class A.

Table 6-1 - Summary of material properties for the test wall simulation

	Material Properties	Value
Concrete	Specific Mass [kg/m^3]	2400
	Moisture Content [kg/m^3]	72
	Convection Coeff. Hot [W/m^{2}K]	25
	Convection Coeff. Cold [W/m^{2}K]	4
	Relative Emission	0.7
	Parameter of Thermal Conductivity	0
	Poisson Ratio	0.2
	Compressive Strength [MPa]	36.1
	Tension Strength [MPa]	2.75
	Strain at Peak Stress	0.0031
	Comp. Damage Peak Stress	0.35
	Tension Ductility [N/m²]	200
Steel	Convection Coeff. Hot [W/m^{2}K]	25
	Convection Coeff. Cold [W/m^{2}K]	4
	Relative Emission	0.7
	Young's Modulus [Gpa]	210
	Poisson Ratio	0.3
	Yield Strength [MPa]	480
	Type	Hot-rolled class A

The temperature analysis is performed on a cross section with the thickness of the wall and an arbitrary width. In this model, the cross section is discretized into 20 elements along the depth of the wall to model its temperature distribution. Reinforcing bars in the shell element are modeled based on a smeared model. The unit area of the reinforcements is assumed to

be a thin sheet of steel in each shell element. The reinforcing layers in the shell elements can have any orientation in the local x–y plane. Each layer is defined by its local vertical coordinate in the shell and the orientation of the reinforcing relative to the local x-axis. Four layers of reinforcing bars are defined here because the mesh consists in one upper layer and one lower layer in each orthogonal direction. In the SAFIR shell element, reinforcements only resist actions parallel to the directions of the reinforcements. Therefore, reinforcements cannot directly resist shear forces. Figure 6-3 shows the discretization of the wall model.

When the thermal analysis is finished, results from the analysis are used to calculate the behavior of this RC wall under fire conditions. Figure 6-3 also shows the temperature distribution of the wall cross section at 90 minutes. It can be seen that the unexposed side of the wall stays unaffected even at the end of the fire exposure time, due to the low thermal conductivity and high thermal capacity of concrete. To verify the validity of this model, the temperature distribution at different time is plotted in figure 6-4. Good agreement can be observed between the numerical results and the test results. It demonstrates the usefulness of modeling the cross-sectional temperature distribution of RC walls with shell elements in SAFIR. It is obvious that the temperature at various depths of concrete, as well as in rebars, increases with fire exposure time. As expected, the predicted temperature decreases with increasing distance from the fire exposed side.

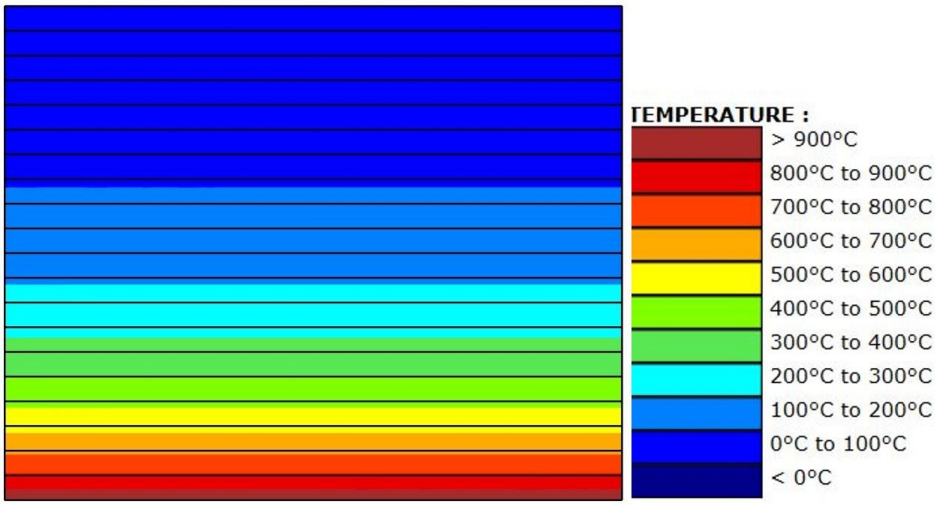

Figure 6-3 - Discretization of the test wall for thermal analysis and temperature distribution at 90 min

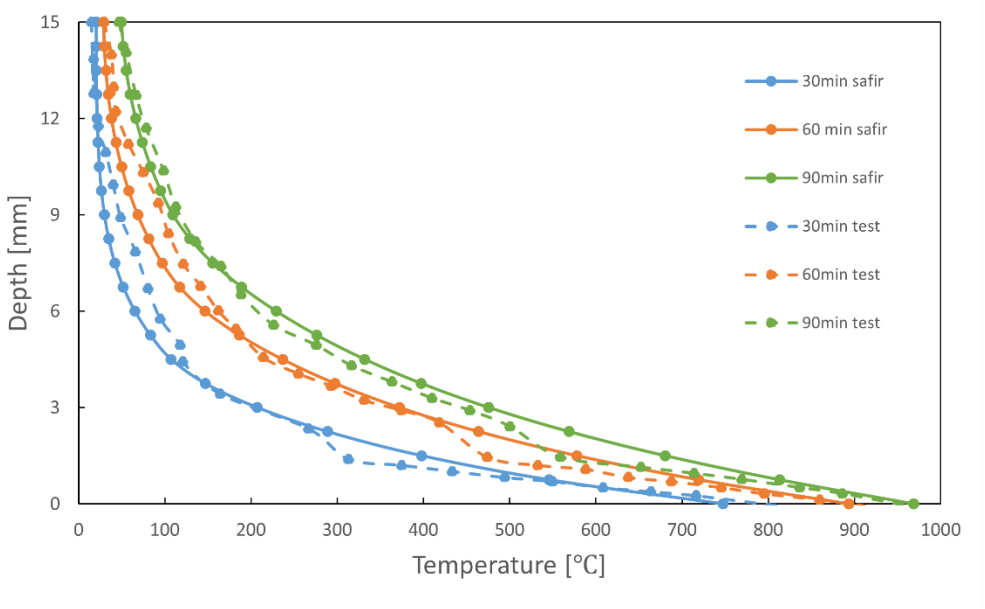

Figure 6-4 - Comparison between test results and numerical results for thermal analysis

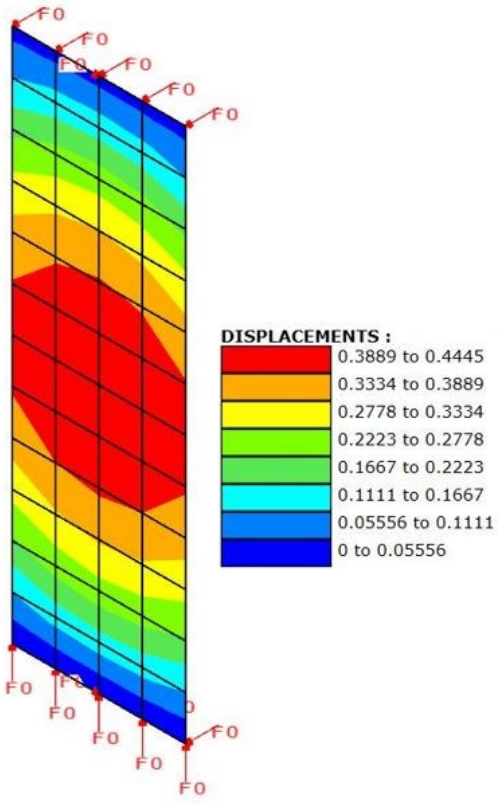

Figure 6-5 - Illustration of the structure model and the out-of-plane displacement at 90 min

The 3D model is created for structural analysis and discretized as shown in figure 6-5. In the test, this wall is hinged at both ends and the top support can move vertically. In the model, the wall is blocked in both x and z axis along the bottom line and x axis along the top line. The y axis is only blocked at the midpoints of both bottom and top lines in order to give room for the wall to expand in y axis under fire exposure. The self-weight is applied as 'Global Shell Load' on each shell element. In order to save computational time, a sensitivity analysis is performed on the mesh size. Finally, a 4*12 mesh (figure 6-5) is chosen. Details of the sensitivity analysis are in the Appendix.

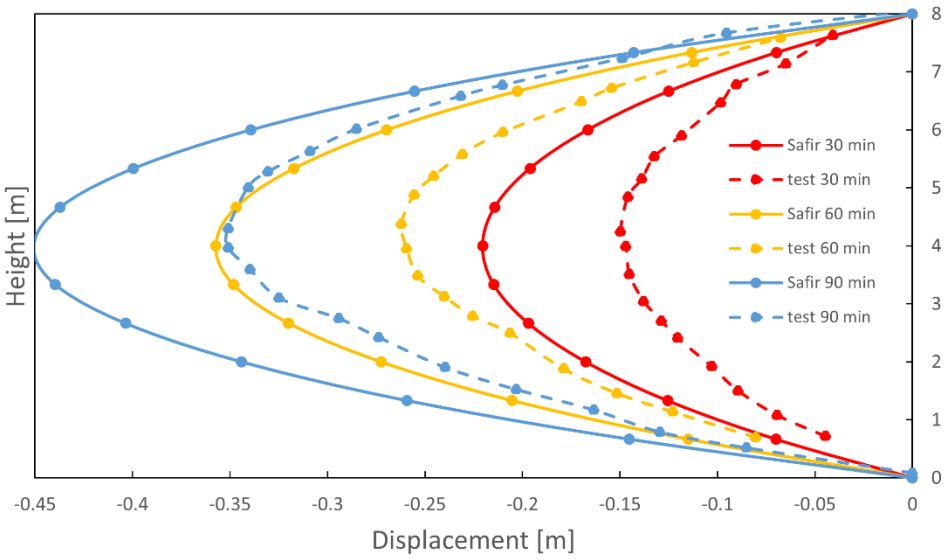

(a) Elevation

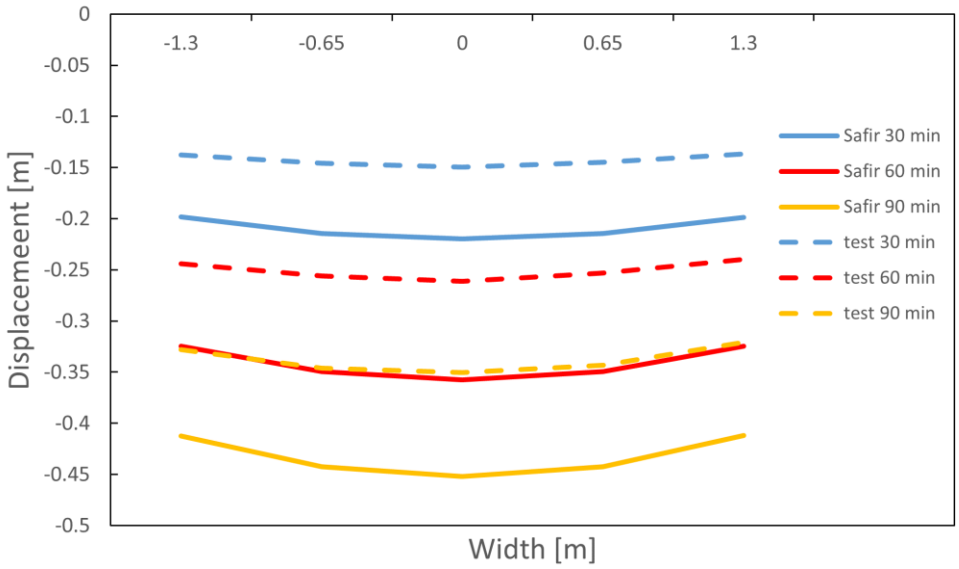

(b) Top view

Figure 6-6 - Deflection shape of the wall (a. elevation, b. top view)

Results of the structural analysis predicted the out-of-plane displacement of the midspan would reach 0.45 m around 90 min of fire exposure. Figure 6-6 shows the evolution of the deflection shape of the midspan during the fire test. The two-way curvature can be observed in the simulation. About one third of the wall surface does not seem significantly affected

by the conditions on these horizontal end supports (where the out-of-plane displacements were kept equal to zero during the test). This may be due to the fact that the width of the wall (2.6 m) is equal to one-third of its height (8.4 m) that is enough to neglect the influence of the two top and bottom edges, while the lateral sides of the wall are stress free. It can also be seen that distribution of displacements is almost symmetrical to the mid-height as well as to the mid-width of the wall. The maximum values appearing in the central zone. The curvatures seem to be slightly decreasing from the central area of the wall to its top and bottom horizontal edges. The out-of-plane displacement modeled by SAFIR is larger than that of the test.

Then the load capacity of this numerical model at ambient temperature is calculated in SAFIR. Five node forces (50N for nodes at the corner and 100N for nodes in the middle; a moment is also applied on each node which equals the applied nodes times L/1000 to simulate the moment caused by the initial imperfection) are applied on all the five nodes at the top with load function ‘F1PS’. This load function allows the total applied load to increase proportionally every second until the structure collapse. Figure 6-7 shows that the wall collapsed around 100 minutes when the total applied load equals 2412 kN (400 N times 6030 sec). Therefore, the load capacity of this wall at ambient temperature is 2412 kN.

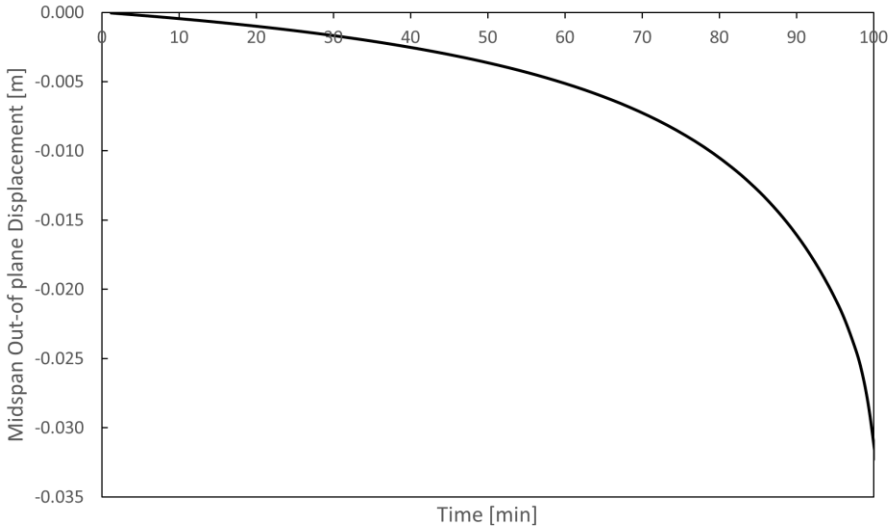

Figure 6-7 – Development of midspan out-of-plane displacement of the wall under the load capacity simulation in SAFIR

6.3 Burnout Resistance Analysis

The burnout resistance of this wall is analyzed in this section. Different load ratios are applied on the wall to see how the wall behaves under standard fire exposures. Load ratio equals the ratio between the load applied on the wall and the load capacity at ambient temperature evaluated by SAFIR, i.e. 2412 kN. Then the burnout resistance analysis is carried out. The process of DHP calculation is the same as for the RC columns and beams. Several thermo-mechanical simulations are iterated until finding the shortest 'natural fire' that leads to failure under the applied load. The iterative method is described in Chapter 3 in detail. However, unlike RC columns and beams that are simulated by beam element, walls simulated by shell elements is hard to converge until the burnout of a natural fire due to its complexity. Therefore, the iterative DHP calculation method is hard to complete automatically by a simple Matlab script. In this study, DHPs are calculated by iterating the

thermo-mechanical analysis manually. The Eurocode parametric natural fire model is used here for the burnout resistance analysis to reduce calculation time. The relationship between DHP and traditional fire resistance is studied. The influence of cooling phase should be studied in the future with a refined RC wall model.

The computed fire burnout resistance, DHP, is given in Table 6-2. The DHP (or burnout resistance) is the shortest duration of the heating phase of the applied natural fire model leading to failure of the column, determined according to the flowchart of Figure 3-1. Figure 6-8 plotted the relationship between R and DHP as computed numerically with SAFIR for the walls under 10 different load ratios.

From Table 6-2, it is observed that such a high-rise wall cannot withstand much loading under one-side fire exposure. The wall would fail in 30 min if it is loaded at only 10% of its normal load capacity. It is due to the large second order effects developing in such a slender vertical element under compressive loading and thermal gradient.

In figure 6-8, DHP increases almost linearly with R and is always smaller than R. A straight line is easily regressed in this figure and fits very well. This phenomenon is very similar to RC columns and walls. We can conclude that, for most concrete structures under given thermal boundary conditions, DHP and R have a linear relationship and the slope depends on the characteristics of the structural collapse.

Table 6-2 - Summary of DHPs for the test RC wall

load ratio	R [min]	DHP [min]
0.01	133	111
0.02	108	91
0.03	88	71
0.04	67	51
0.05	54	37
0.06	45	27
0.07	38	22
0.08	32	17
0.09	29	12
0.1	26	10

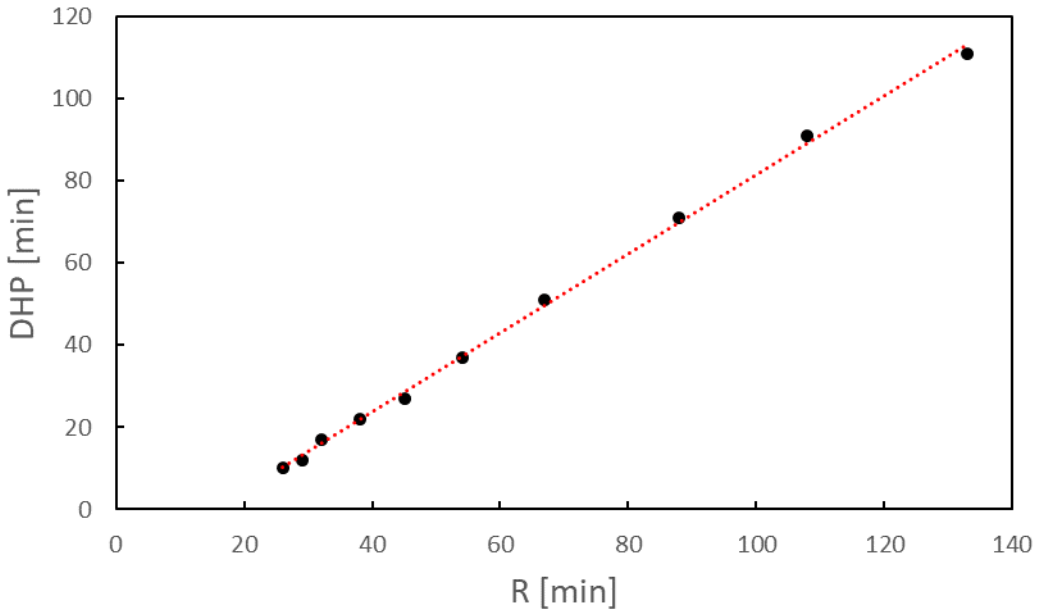

Figure 6-8 – DHP-R relationship for the RC wall

6.4 A Data-based Equation for RC Wall DHP Calculation

This section aims at deriving an equation to relate DHP directly as a function of R. Since the wall is analyzed under Eurocode parametric natural fire model, Eq. 4-1 proposed by Gernay [5] for RC columns is firstly applied to see if the equation for columns can predict

the DHP of wall accurately. Figure 6-9 compares the results predicted by Eq. 4-1 with the real DHPs got from SAFIR. It can be seen that the DHPs for this wall does not agree well with the equation for columns probably because of the large second order effects of such a high wall and transverse bending of walls under fire exposure.

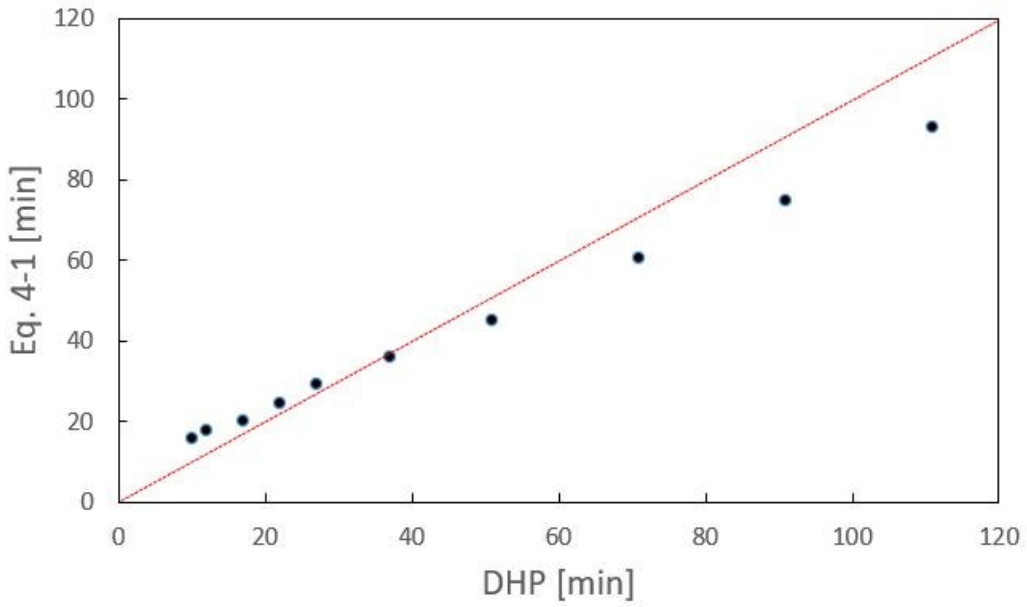

Figure 6-9 Comparison between DHP and the results calculated by Eq. 4-1

However, examination of the results of Table 6-2 demonstrates that the DHP does have a linear relationship with R. Thus, a linear regression on the data of Table 6-2 is performed to derive a very simple formulation of Eq. 6-1, with a R squared value of 0.998:

$$DHP = 0.96R-14.77 \quad (6\text{-}1)$$

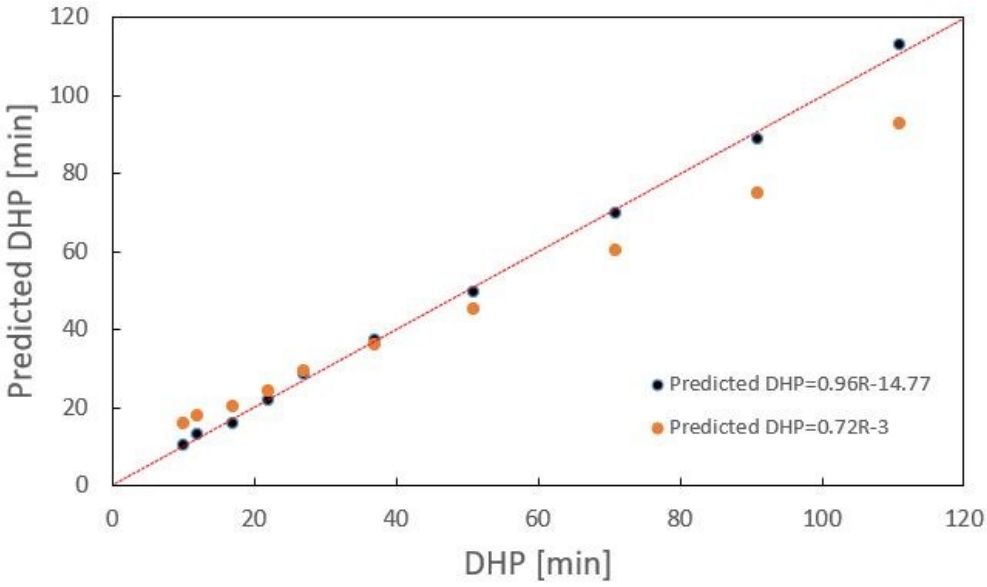

Figure 6-10 Comparison between DHP and the results calculated by Eq. 6-1

This equation yields the DHP directly as a function of R. Fig. 6-10 plots the DHP estimated by Eq. 6-1 where the R is taken from the SAFIR model, against the DHP computed directly by SAFIR. Good agreement is clearly observed, which proves the usefulness of this equation and can save a lot of computational time on calculating burnout resistance. However, more tests are still needed to validate the applicability of this equation on other high-rise walls or other normal RC walls.

7. General Conclusions

7.1 Discussion

The burnout resistance (DHP) is an extension of the traditional fire resistance rating (R) concept to account for the effects of cooling down phases of natural fires on the load-bearing capacity and stability of structural members. A standardized natural fire model is proposed for a systematic burnout resistance analysis. The burnout resistance analysis is performed on concrete columns, beams and a high-rise wall using SAFIR to investigate the factors that influence the burnout resistance (DHP).

Based on the results, the value of DHP is closely related to the fire resistance R and cooling rate K. The DHP of a member increases with an increase in R (greater fire resistance) and in K (faster cooling). A structure with a high fire resistance R obviously has a high DHP, although the coefficient of proportionality is smaller than one meaning that increases in R translates into smaller gains in burnout resistance. In terms of K, it also has a great influence on the value of DHP especially when the R of a structure is large and the cooling rate K is slow.

It should be noticed that the couple of DHP and R can also inform the propensity of a structure to exhibit delayed failure under a designed natural fire. When DHP and R are close, the structure is unlikely to fail during or after the cooling phase of a fire. If such a member is still standing when the firefighters start extinguishing the fire, the most likely outcome is that it will survive full burnout. In contrast, structural members with a DHP much shorter than their fire resistance is at risk of delayed failure. Members with DHP and R ratings that are very different are disadvantageous as they are prone to delayed failures.

Therefore, in practical design, when a structure needs to be designed with high standard fire resistance, it is necessary to consider the possibility of delayed failure during the cooling phase since the value of DHP may change greatly and even make the structure fail to meet the design objectives.

For RC columns, several strategies based on equal area method, maximum temperature method, and load capacity approaches are checked to define equivalent fire severity to infer structural behavior under realistic fire exposure from standard fire resistance ratings. As a result, none of these simple strategies can fit all the columns tests well since the behavior of concrete columns under fire exposure depends on various factors. When the equal area method is applied, the area of the temperature-time curve decreases slowly when the cooling rate increases. It is probably because the area of the fire curve essentially does not have any theoretical meaning and the radiative heat transfer is proportional to the fourth power of the absolute temperature, heat transfer to the surface in a short hot fire may be much greater than in a long cool fire. In terms of the maximum temperature method, the maximum corner rebar temperature is selected for simplicity. This method fits a sample of the tests (with high fire resistance) reasonably well. However, for others (mostly tests with low fire resistance), the rebar remains its full strength even if it reaches its maximum temperature probably due to a different failure mode. For the load capacity method, iso500therm method is applied. The load capacities of the tested column at failure under different fire exposure fluctuate around the load capacity at failure under ISO 834 fire curve since the iso500therm method is not accurate enough. It is also interesting to notice that the equivalent fire severity concept does not work well in all the 3 strategies above when the cooling rate is slow. More research is needed to explore the behavior of concrete

structures under a natural fire with a slow cooling rate. Therefore, a simple strategy of equivalent fire severity cannot be used to evaluate whether a RC column would survive a fire; it is necessary to consider the thermal-structural response (or a design equation calibrated on finite element results). It is interesting and noteworthy to see whether some more complex strategies can be applied to define the equivalent fire severity. For beams, the maximum temperature method is applied for equivalent fire severity. Unlike concrete columns, the method is applicable for beams. The maximum rebar temperatures are around the maximum rebar temperature of ISO834 fire test with a little variation. This might be due to the fact that the bending failure of beams is mostly caused by yield of reinforcements while the concrete still has large influence on the compression failure of columns.

Finally, based on the numerical dataset, simple equations could be regressed to evaluate the DHP from the given R and K for beams and columns. For the wall, DHP is only regressed as a function of R because it is analyzed under the Eurocode natural fire model; further research is needed to explore the effect of K. The simple form of the data-base equation is an advantage for the practical purpose since the burnout resistance is directly calculated from the fire resistance and cooling rate. Thus, for practical application, the recommendation is that the prescriptive classification of structural members could rely on a pair of metrics (DHP, R) rather than on the fire resistance only. These two metrics taken together provide a more complete picture of the structural response under the different stages of a fire until complete burnout and, in combination, they inform on the vulnerability to delayed structural failure. For reinforced concrete columns and beams, engineers can simply estimate the DHP using the derived equations. Therefore, this new metric is a good way to quantify the ability of a structure to survive full burnout. However, it should be

noticed that we cannot conclude that a real compartment fire that lasts shorter than the DHP of the structure will not lead to eventual collapse, because real compartment fires are still different from the standardized fire model considered in the research. In the future, investigations will focus on other member typologies and materials to derive the burnout resistance, and it will be interesting to discover whether the linear relation between R and DHP still holds true.

7.2 Conclusions

The standard fire resistance metrics has proven to be very useful in structural fire engineering over the past decades and continues to have its place nowadays alongside the more sophisticated performance-based approaches. However, this traditional metric still can be improved. The definition of DHP is a good example. It is an extension of traditional fire resistance and has been proven in previous research to be a useful and simple way to access the possibility of delayed failure during the cooling phase. In practical design, engineers can easily access the behavior of concrete structures under a natural fire by adopting the DHP metrics.

This research investigated the factors that influence the value of DHP. Therefore, this research compiled a database of 74 standard fire resistance tests for columns, 2 type of beams and a high-rise wall. In a first step, a standardized natural fire model was created with a uniform heating phase and variable cooling rates. The range of realistic cooling rate is then confirmed by numerous OZone numerical tests.

In a second step, these concrete columns and beams were analyzed under the standardized natural fire model and the walls were analyzed under Eurocode natural fire model by

numerical software. An iterative computational procedure using half-interval search method was applied to each member until finding the shortest fire that could not be survived until burnout, hence determining the DHP, or burnout resistance, of each column. It was found that the cooling rate has a great influence on the burnout resistance of concrete columns. In other words, the difference between DHP and R will be greatly influenced by the cooling rate, which is a good indicator of the possibility of delayed failure. The equivalent fire severity concept was explored by adopting several simple methods but none of them can fit all the column tests well due to the complex behavior of the concrete column under natural fire exposure. However, for beams, the maximum rebar temperature method fits the test well.

Finally, simple equations was then regressed from the obtained dataset to estimate the burnout resistance DHP for concrete structures. This equation allows a straightforward evaluation of the DHP for reinforced concrete members at no additional cost. Providing an easy method for estimating the burnout resistance is important because designing for complete burnout has benefits for the safety of fire brigades and first responders, as well as for property protection and resilience of the built environment. This research has applied a novel methodology to the case of reinforced concrete members, but in the future other structural members and materials should be investigated to evaluate their burnout resistance. The DHP could be generalized to any structure and serve the profession well as a complement to the current fire-resistance rating in the prescriptive approach.

Acknowledgement

The research work presented in this thesis has been supported by the ACI Foundation through research grant # CRC 2020 P0039 awarded to Dr. Thomas Gernay. This support is gratefully acknowledged.

References

[1] ISO 834-1975 Organization International for Standardization, Fire Resistance Tests- Elements of Building Construction, 1975.

[2] American Society for Testing and Materials, ASTM Standard Methods of Fire Test of Building Construction and Materials, 2008. Test Method E119a -08, West Conshohocken, PA.

[3] A. Muttoni, A.A. Furst, F. Hunkeler, November, Medieninformation vom15, Deckeneinsturzder Tiefgarageam Staldenacker in Gretzenbach vol. 11, Solothurn, Switzerland, 2005.

[4] Gernay, T., Franssen, J. M. A performance indicator for structures under natural fire. Engineering Structures, 100, 94-103, 2015.

[5] Gernay, T. Fire resistance and burnout resistance of reinforced concrete columns. Fire safety journal, 104, 67-78, 2019.

[6] T. Thienpont, R. Van Coile, R. Caspeele, W. De Corte, Comparison of fire resistance and burnout resistance of simply supported reinforced concrete slabs exposed to parametric fires, in: Proc. CONFAB 2019, London, 2019.

[7] Gernay, T. (2021). Fire Resistance and Burnout Resistance of Timber Columns. *Fire Safety Journal*, 103350.

[8] J-F. Cadorin, J-M. Franssen, A tool to design steel elements submitted to compartment fires—OZone V2. Part 1: pre- and post-flashover compartment fire model, Fire Safety Journal 38, 395–427, 2003.

[9] J-F. Cadorin*, D. Pintea, J-C. Dotreppe, J-M. Franssen, A tool to design steel elements submitted to compartment fires—OZone V2. Part 2: Methodology and application, Fire Safety Journal 38, 429–451, 2003.

[10] EN 1994-1-2, Eurocode 4 - Design of composite steel and concrete structures - Part 1-2: General rules - Structural fire design, CEN, Brussels, 2005.

[11] EN 1992-1-2, Eurocode 2 – Design of Concrete Structures. Part 1–2: General Rules – Structural Fire Design, CEN, Brussels, 2004.

[12] ÉPERNON FIRE TESTS PROGRAMME SYNTHESIS REPORT, EFTP,2020. http://www.epernon-fire-tests.eu/

[13] Bartlett, A. I., McNamee, R., Robert, F., & Bisby, L. A. (2020). Comparative energy analysis from fire resistance tests on combustible versus noncombustible slabs. *Fire and Materials*, *44*(3), 301-310.

[14] R. Haß, Zur praxisgerechten brandschutztechnischen Beurteilung von Stützen aus Stahl und Beton vol. 69, Inst. für Baustoffe, Massivbau und Brandschutz der Technishen Universität Braunschweig, 1986 Heft.

[15] J.C. Dotreppe, J.M. Franssen, A. Bruls, R. Baus, P. Vandevelde, R. Minne, D. Van Nieuwenburg, H. Lambotte, Experimental research on the determination of the main parameters affecting the behaviour of reinforced concrete columns under fire conditions, Mag. Concr. Res. 49 (179) (1997) 117–127.

[16] T.T. Lie, J.L. Woollerton, Fire Resistance of Reinforced Concrete Columns: Test Results, National Research Council of Canada, Institute for Research in Construction, Ottawa, Canada, 1988.

[17] J.M. Franssen, T. Gernay, Modeling structures in fire with SAFIR® : theoretical background and capabilities, Journal of Structural Fire Engineering 8 (3) (2017) 300–323.

[18] T. Gernay, J.M. Franssen, A formulation of the Eurocode 2 concrete model at elevated temperature that includes an explicit term for transient creep, Fire Saf. J. 51 (2012) 1–9.

[19] EN 1992-1-2, Eurocode 2 – Design of Concrete Structures. Part 1–2: General Rules – Structural Fire Design, CEN, Brussels, 2004.

[20] L. Yi-Hai, J.M. Franssen, Test results and model for the residual compressive strength of concrete after a fire, J Struct Fire Eng 2 (1) (2011) 29–44.

[21] B.R. Kirby, D.G. Lapwood, G. Thomson, The Reinstatement of Fire Damaged Steel and Iron Framed Structures, B.S.C., Swinden Laboratories, London, UK, 1986 0900206 46 2.

[22] Zhan-Fei Huang, Kang-Hai Tan, Rankine approach for fire resistance of axially and flexurally restrained steel columns, J. Constr. Steel Res. 59 (12) (2003) 1553–1571.

[23] A. Espinos, M.L. Romero, A. Hospitaler, Advanced model for predicting the fire response of concrete filled tubular columns, J. Constr. Steel Res. 66 (8–9) (2010) 1030–1046.

[24] Ingberg, Tests of the severity of building fires, 1928.

[25] Law M. A Review of Formulae for T-Equivalent. Fire Safety Science, Proceedings of the Fifth International Symposium, pp. 985–996, International Association for Fire Safety Science, 1997.

[26] Lane B. Performance-Based Design for Fire Resistance. Modern Steel Construction, 2000.

[27] Buchanan. A. H., Aba A. K. Structural Design for Fire Safety. Second Edition. John Wiley & Sons, Ltd. 2017.

[28] Ana Sauca. Development and implementation of a methodology for hybrid fire testing applied to concrete structures with elastic boundary conditions. Ph. D. thesis, University of Liege, 2016.

[29] Kodur V.K.R., Dwaikat M. A numerical model for predicting the fire resistance of reinforced concrete beams. Cement & Concrete Composites, 30, 431–443, 2008.

[30] ACI Committee 2161. Standard method for determining fire resistance of concrete and masonry construction assemblies. Detroit: American Concrete Institute; 1997.

[31] Pham D. T., Pinoteau N., Yang Mingguan et al. Full-scale fire test on a high-rise RC wall. Engineering Structures, 227, 111435, 2021.

[32] Franssen JM. SAFIR: a thermal/structural program modelling structures under fire. Proceedings of the North American Steel Construction Conference, April, A.I.S.C. Inc., Baltimore,2003.

[33] Lim L., Buchanan A., Mossb P., Franssen J. M. Numerical modelling of two-way rein forced concrete slabs in fire. Engineering Structures, 26, 1081–1091, 2004.

[34] Gernay, T., Millard, A., & Franssen, J. M. (2013). A multiaxial constitutive model for concrete in the fire situation: Theoretical formulation. *International Journal of Solids and Structures*, *50*(22-23), 3659-3673.

[35] Gernay, T., & Franssen, J. M. (2015). A plastic-damage model for concrete in fire: Applications in structural fire engineering. Fire Safety Journal, *71*, 268-278.

Appendix

Mesh sensitivity and load capacity for RC wall

The mesh sensitivity analysis is conducted to both save computational time and see enough displacement details of the wall. In this analysis, the mesh size changed from 2*4 to 12*48. The load capacity at ambient temperature and midpoint displacement is used as two factors to justify if this mesh size is accurate enough to capture the structural behavior. A dataset of this analysis is summarized as follow:

Mesh size	Load Capacity at ambient temperature [kN]	Displacement at middle point under ISO834 at 90 min [m]
2*4	2412	0.4653
4*12	2406	0.4522
4*16	2390	0.4561
6*18	2412	0.4555
6*24	2412	0.4561
8*24	2410	0.4534
10*40	2376	0.4568
12*36	2408	0.4546
12*48	2404	0.4574

From the table above, we can see that the load capacity and the midpoint displacements does not change greatly even if the mesh size is very different. That means the mesh size does not have much influence on the wall simulation. Therefore, in this research, a 4*12 mesh is selected which can both capture the structural behavior accurately and get enough detail for the deflection shape comparison.